Thermally-actuated shape-memory polymers: experiments, theory, and numerical simulations

Vikas Srivastava, Shawn A. Chester, and Lallit Anand*
Department of Mechanical Engineering
Massachusetts Institute of Technology
Cambridge, MA 02139, USA

July 26, 2011

Abstract

With the aim of developing a thermo-mechanically-coupled large-deformation constitutive theory and a numerical-simulation capability for modeling the response of thermally-actuated shape-memory polymers, we have (i) conducted large strain compression experiments on a representative shape-memory polymer to strains of approximately unity at strain rates of 10^{-3} s^{-1} and 10^{-1} s^{-1}, and at temperatures ranging from room temperature to approximately 30 C above the glass transition temperature of the polymer; (ii) formulated a thermo-mechanically-coupled large-deformation constitutive theory; (iii) calibrated the material parameters appearing in the theory using the stress-strain data from the compression experiments; (iv) numerically implemented the theory by writing a user-material subroutine for a widely-used finite element program; and (v) conducted representative experiments to validate the predictive capability of our theory and its numerical implementation in complex three-dimensional geometries. By comparing the numerically-predicted response in these validation simulations against measurements from corresponding experiments, we show that our theory is capable of reasonably accurately reproducing the experimental results. As a demonstration of the robustness of the three-dimensional numerical capability, we also show results from a simulation of the shape-recovery response of a stent made from the polymer when it is inserted in an artery modeled as a compliant elastomeric tube.

1 Introduction

The most common shape-memory polymers are those in which the shape-recovery is *thermally-induced* (e.g., Behl and Lendlein, 2007; Ratna and Kocsis, 2008).[1] A body made from such a material may be subjected to large deformations at an elevated temperature above its glass transition temperature ϑ_g. Cooling the deformed body to a temperature below ϑ_g under active kinematical constraints fixes the deformed shape of the body. The original shape of the body may be recovered if the material is heated back to a temperature above ϑ_g without the kinematical constraints. This phenomenon is known as the *shape-memory effect*. If the shape recovery is partially constrained, the material exerts a recovery force and the phenomenon is known as *constrained-recovery*.

As reviewed by Gall et al. (2005), one of the first widespread applications of shape-memory polymers was as heat-shrinkable tubes (Ota, 1981). Such rudimentary early applications did not necessitate a detailed understanding or modeling of the thermomechanical behavior of these materials. However, in recent years shape-memory polymers are beginning to be used for critical biomedical applications (e.g., Lendlein and

*Corresponding author. Tel.: +1-617-253-1635; E-mail address: anand@mit.edu

[1] Shape-memory polymers which can recover from an imposed deformation by the application of other external stimuli such as light of a specific frequency also exist (e.g., Lendlein et al., 2005; Jiang et al., 2006). However, in this study we limit our attention to thermally-actuated shape-memory polymers.

Langer, 2002; Metcalfe et al., 2003; Baer et al., 2007b), microsystems (e.g., Maitland et al., 2002; Metzger et al., 2002; Gall et al., 2004), re-writable media for data storage (e.g., Vettiger et al., 2002; Wornyo et al., 2007), and self-deployable space structures (Campbell et al., 2005). In order to develop a robust simulation-based capability for the design of devices for such critical applications, one requires an underlying accurate thermo-mechanically-coupled constitutive theory and an attendant validated numerical implementation of the theory.

In the past few years several efforts at experimental characterization of the thermo-mechanical stress-strain response of a wide variety of shape-memory polymers have been published in the literature (e.g., Tobushi et al., 1996; Baer et al., 2007a; Gall et al., 2005; Yakacki et al., 2007; Safranski and Gall, 2008; Qi et al., 2008). Significant modeling efforts have also been published (e.g., Liu et al., 2006; Chen and Lagoudas, 2008; Qi et al., 2008; Nguyen et al., 2008). However, at this point in time, a thermo-mechanically-coupled large-deformation constitutive theory for modeling the response of thermally-actuated shape-memory polymers is not widely agreed upon — the field is still in its infancy. The purpose of this paper is to present results from of our own recent research in this area.

Specifically, with the aim of developing a thermo-mechanically-coupled large-deformation constitutive theory and a numerical simulation capability for modeling the response of thermally-actuated shape-memory polymers, we have

(i) conducted large strain compression experiments on a representative shape-memory polymer to strains of approximately unity at strain rates of 10^{-3} s^{-1} and 10^{-1} s^{-1}, and at temperatures ranging from room temperature to approximately 30 C above the glass transition temperature of the polymer;

(ii) formulated a thermo-mechanically-coupled large deformation constitutive theory;

(iii) calibrated the material parameters appearing in the theory using the stress-strain data from the compression experiments;

(iv) numerically implemented the theory by writing a user-material subroutine for a widely-used finite element program ABAQUS/Standard (2009); and

(v) conducted representative experiments to validate the predictive capability of our theory and its numerical implementation in complex three-dimensional geometries. By comparing the numerically-predicted response in these validation simulations against measurements from corresponding experiments, we show that our theory is capable of reasonably accurately reproducing the experimental results.

Also, as a demonstration of the robustness of the three-dimensional numerical capability, we show results from a simulation of the shape-recovery response of a stent made from the polymer when it is inserted in an artery modeled as a compliant elastomeric tube.

The plan of this paper is as follows. In §2 we describe results of our simple compression experiments on a representative chemically-cross-linked *thermoset* shape-memory polymer. In §3 we summarize our constitutive theory, and show the quality of the fit of the constitutive theory to the experimentally-measured stress-strain curves. For ease of presentation, the details of the specialization of the constitutive theory to model the particular shape-memory polymer used in our study are discussed in an Appendix. In §4 we present experimental results and corresponding numerical simulations from our validation study. We close in §5 with some final remarks.

2 Experimental characterization of the thermo-mechanical response of a shape-memory polymer

As a representative thermally-actuated shape-memory polymer we chose to characterize the mechanical response of a chemically-crosslinked thermoset polymer recently studied by Yakacki et al. (2007). Following a procedure described by these authors, the shape-memory polymer was synthesized via photopolymerization (UV curing) of the monomer tert-butyl acrylate (tBA) with the crosslinking agent poly(ethylene glycol) dimethacrylate (PEGDMA), in the following specific composition: tBA 90% by weight (mol. weight: 128

g/mol) with PEGDM 10% by weight (mol. weight: 550 g/mol).[2] This polymer is chosen for study because the shape-memory actuation temperature for this polymer is close to that of body-temperature — the *nominal* glass transition temperature for this polymer is $\vartheta_g \approx 37\,\mathrm{C}$ (Safranski and Gall, 2008).

We have conducted a set of simple compression experiments on this polymer. The cylindrical specimens were 6.3 mm diameter and 3.15 mm tall. The compression experiments were conducted at true-strain rates of 10^{-3} s^{-1} and 10^{-1} s^{-1} at 22 C, 30 C, 40 C, 50 C, and 65 C, up to true strain-levels of $\approx 100\%$. Fig. 1 shows representative true stress-strain curves.[3] The polymer exhibits two distinctly different responses at temperatures below and above ϑ_g:

- The stress-strain curves at 22 C and 30 C are below ϑ_g. At these temperatures the polymer exhibits a strain-rate and temperature-dependent response typical of a "glassy-polymer". That is, a well-defined yield-peak, followed by strain-softening, and eventual rapid strain-hardening at large strains. Upon unloading after compression to a strain level of $\approx 100\%$, about 5% of the strain is recovered and the remainder is left as a "permanent-set" (as long as the temperature is held constant).

- The stress-strain curves at 50 C and 65 C are above ϑ_g. At these temperatures the material exhibits a "hysteretic-rubber"-like response. That is, the initial stiffness of the material drops dramatically from its value below ϑ_g, the yield-peak disappears, and upon unloading there is essentially no permanent set. However, there is significant hysteresis in the stress-strain response which is significantly rate- and temperature-dependent.

Of particular interest are the two stress-strain curves at 40 C, a temperature which is in the vicinity of the *nominal* glass transition temperature of $\vartheta_g \approx 37\,\mathrm{C}$. At the lower strain rate of $10^{-3}\,\mathrm{s}^{-1}$ the material responds like a "hysteretic-rubber", while at the higher strain rate of $10^{-1}\,\mathrm{s}^{-1}$ the material responds like a "glassy-polymer." Thus, in accordance with the well-known result from frequency-dependent dynamic-mechanical-tests on amorphous polymers, this result shows that the "glass transition temperature" ϑ_g is *not a constant* for a material — it increases as the strain rate increases.

3 Constitutive theory

Amorphous polymers are called *thermoplastics* when they are not chemically-crosslinked, and are called *thermosets* when they are chemically-crosslinked. Both classes of amorphous polymers behave in a qualitatively similar fashion when deformed below ϑ_g, but their response characteristics above ϑ_g are quite different. As shown in Fig. 1, at temperatures above ϑ_g, after a certain amount of deformation, the crosslinked thermoset material recovers almost fully upon reverse deformation – *a response essential to the shape-memory effect*. Unlike a crosslinked thermoset polymer, an amorphous polymer which is not crosslinked shows *permanent set* when subjected to a strain-cycle above ϑ_g, and is therefore said to be "thermoplastic" in character.

Over the past thirty years, considerable effort has been devoted to developing constitutive models to represent the large-deformation elastic-viscoplastic behavior of *amorphous thermoplastic polymers* (cf., e.g., Parks et al., 1985; Boyce et al., 1988; Buckley and Jones, 1995; Boyce et al., 2000; Govaert et al, 2000; Dooling et al., 2002; Anand and Gurtin, 2003; Anand and Ames, 2006; Dupaix and Boyce, 2007). These models have been primarily used to describe the *isothermal* deformation of these polymers below their glass transition temperatures. In a recent pair of papers (Anand et al., 2009; Ames et al., 2009) we have developed a *thermo-mechanically-coupled* large-deformation theory for amorphous thermoplastic materials; however, this theory is limited to a temperature range below the glass transition temperatures of such materials. Very recently, we have extended this theory to model the response of amorphous thermoplastic polymers in a temperature range which *spans* their glass transition temperature (Srivastava et al., 2009). For modeling the response of *amorphous thermoset shape-memory polymers*, we adopt and adapt the constitutive framework of Srivastava et al.. In what follows we summarize our constitutive framework, but relegate the specialization of the theory

[2] The chemicals were mixed in a glass beaker for 2 minutes, and the mixed liquid solution was then degassed in a vacuum chamber for 10 minutes. The degassed mixture was then injected between two glass sheets that were separated with spacers. A UV-Lamp was used to photopolymerize the solution at an intensity of $\sim 30\,\mathrm{mW/cm^2}$ for 10 minutes. Finally, the polymer was heat-treated at 90 C for 1 hour to complete the polymerization reaction.

[3] As is customary, in order to calculate the deformed cross-sectional area (and thence the true stress), we have assumed plastic incompressibility to estimate the stretch in the lateral direction of the compression specimens.

to model shape-memory polymers and the specific application to model the response of tBA/PEGDMA to an Appendix.

An essential kinematical ingredient of elastic-viscoplastic constitutive theories for amorphous polymers *below their glass transition temperatures* is the classical Kröner (1960) – Lee (1969) multiplicative decomposition[4]

$$\mathbf{F} = \mathbf{F}^e\mathbf{F}^p, \qquad \text{with} \qquad \det\mathbf{F}^e > 0 \quad \text{and} \quad \det\mathbf{F}^p > 0, \tag{3.1}$$

of the deformation gradient $\mathbf{F}$ into elastic and plastic parts $\mathbf{F}^e$ and $\mathbf{F}^p$ (e.g., Boyce et al., 1988; Govaert et al, 2000; Anand and Gurtin, 2003; Anand et al., 2009). Since we wish to model the behavior of polymers in the technologically important temperature range which *spans* their glass transition temperatures, and since the number of microscopic relaxation mechanisms in these polymers increases as the temperature is increased, we base our theory on a "multimechanism" generalization of the decomposition (3.1),

$$\mathbf{F} = \mathbf{F}^{e\,(\alpha)}\mathbf{F}^{p\,(\alpha)}, \qquad \text{with} \qquad \det\mathbf{F}^{e\,(\alpha)} > 0 \quad \text{and} \quad \det\mathbf{F}^{p\,(\alpha)} > 0, \qquad \alpha = 1,\dots,M, \tag{3.2}$$

where each α denotes a local micromechanism of deformation. Such a multi-mechanism generalization forms the basis of the work of Buckley, Boyce, and their co-workers (e.g., Buckley and Jones, 1995; Bergstrom and Boyce, 1998; Boyce et al., 2000; Dooling et al., 2002; Dupaix and Boyce, 2007). For each micromechanism indexed by α, we refer to $\mathbf{F}^{p\,(\alpha)}$ and $\mathbf{F}^{e\,(\alpha)}$ as the *plastic and elastic parts* of $\mathbf{F}$.

In what follows, when summing quantities over the M micro-mechanisms, we used the shorthand

$$\sum_{\alpha} \equiv \sum_{\alpha=1}^{M}.$$

REMARK 1. In a one-dimensional theory of linear viscoelasticity, which is based on a widely-used mechanical analog of M Maxwell-elements assembled in parallel, the one-dimensional strain ϵ is decomposed as

$$\epsilon = \epsilon^{e(\alpha)} + \epsilon^{p(\alpha)}, \qquad \alpha = 1,\dots,M;$$

the decomposition (3.2) is a three-dimensional, large-deformation, generalization of such a decomposition.

Restrict attention to a prescribed *material point* $\mathbf{X}$, and let $\mathbf{x}$ denote its place in the deformed configuration at a fixed time t. Then, bearing in mind that (for $\mathbf{X}$ fixed) the linear transformations $\mathbf{F}^{e\,(\alpha)}(\mathbf{X})$ and $\mathbf{F}^{p\,(\alpha)}(\mathbf{X})$ at $\mathbf{X}$ are invertible, we let

$$\mathcal{M}_{\mathbf{X}}{}^{(\alpha)} \stackrel{\text{def}}{=} \text{range of } \mathbf{F}^{p\,(\alpha)}(\mathbf{X}) = \text{domain of } \mathbf{F}^{e\,(\alpha)}(\mathbf{X}), \tag{3.3}$$

and refer to $\mathcal{M}_{\mathbf{X}}{}^{(\alpha)}$ as the *intermediate structural space* at $\mathbf{X}$ for the α-th micromechanism. Even though we use this terminology, *there is no actual physical space* that may be associated with an "intermediate structural space" — such a space is a purely mathematical construct.

Also, it is important to note from the outset, that each $\mathbf{F}^{p\,(\alpha)}$ is to be regarded as an internal variable of the theory which is defined as a solution of the differential equation (the *flow rule* to be discussed shortly)

$$\dot{\mathbf{F}}^{p\,(\alpha)} = \mathbf{D}^{p\,(\alpha)}\mathbf{F}^{p\,(\alpha)} \quad \text{with} \quad \det\mathbf{F}^{p\,(\alpha)} = 1, \quad \text{and with initial condition} \quad \mathbf{F}^{p\,(\alpha)}(\mathbf{X},0) = \mathbf{1}. \tag{3.4}$$

The corresponding $\mathbf{F}^{e\,(\alpha)}$ is then defined by $\mathbf{F}^{e\,(\alpha)} \stackrel{\text{def}}{=} \mathbf{F}\mathbf{F}^{p\,(\alpha)-1}$. Hence the decompositions (3.2) are not purely kinematical in nature as they are not defined independently of constitutive equations; they are to be viewed as *kinematical constitutive equations*.

Our theory relates the following basic fields:

[4]Notation: We use standard notation of modern continuum mechanics (e.g., Gurtin, Fried, and Anand, 2009). Specifically: ∇ and Div denote the gradient and divergence with respect to the material point $\mathbf{X}$ in the reference configuration; grad and div denote these operators with respect to the point $\mathbf{x} = \boldsymbol{\chi}(\mathbf{X},t)$ in the deformed body; a superposed dot denotes the material time-derivative. Throughout, we write $\mathbf{F}^{e-1} = (\mathbf{F}^e)^{-1}$, $\mathbf{F}^{p-\top} = (\mathbf{F}^p)^{-\top}$, etc. We write $\operatorname{tr}\mathbf{A}$, $\operatorname{sym}\mathbf{A}$, $\operatorname{skw}\mathbf{A}$, $\mathbf{A}_0$, and $\operatorname{sym}_0\mathbf{A}$ respectively, for the trace, symmetric, skew, deviatoric, and symmetric-deviatoric parts of a tensor $\mathbf{A}$. Also, the inner product of tensors $\mathbf{A}$ and $\mathbf{B}$ is denoted by $\mathbf{A}:\mathbf{B}$, and the magnitude of $\mathbf{A}$ by $|\mathbf{A}| = \sqrt{\mathbf{A}:\mathbf{A}}$.

$\mathbf{x} = \boldsymbol{\chi}(\mathbf{X}, t)$,	motion;
$\mathbf{F} = \nabla\boldsymbol{\chi}, \quad J = \det\mathbf{F} > 0$,	deformation gradient;
$\mathbf{F} = \mathbf{F}^{e\,(\alpha)}\mathbf{F}^{p\,(\alpha)}, \quad \alpha = 1, \ldots, M$,	elastic-plastic decompositions of $\mathbf{F}$;
$\mathbf{F}^{e\,(\alpha)}, \quad J^{e\,(\alpha)} = \det\mathbf{F}^{e\,(\alpha)} = J > 0$,	elastic distortions;
$\mathbf{F}^{p\,(\alpha)}, \quad J^{p\,(\alpha)} = \det\mathbf{F}^{p\,(\alpha)} = 1$,	inelastic distortions;
$\mathbf{F}^{e\,(\alpha)} = \mathbf{R}^{e\,(\alpha)}\mathbf{U}^{e\,(\alpha)}$,	polar decompositions of $\mathbf{F}^{e\,(\alpha)}$;
$\mathbf{C}^{e\,(\alpha)} = \mathbf{F}^{e\,(\alpha)\top}\mathbf{F}^{e\,(\alpha)}$,	elastic right Cauchy-Green tensors;
$\mathbf{B}^{p\,(\alpha)} = \mathbf{F}^{p\,(\alpha)}\mathbf{F}^{p\,(\alpha)\top}$,	plastic left Cauchy-Green tensors;
$\mathbf{T} = \sum_\alpha \mathbf{T}^{(\alpha)}, \qquad \mathbf{T}^{(\alpha)} = \mathbf{T}^{(\alpha)\top}$,	Cauchy stress;
$\mathbf{T}_{\mathrm{R}} = J\mathbf{T}\mathbf{F}^{-\top}$,	Piola stress;
$\psi_{\mathrm{R}} = \sum_\alpha \bar{\psi}^{(\alpha)}$,	free energy density per unit reference volume;
$\eta_{\mathrm{R}} = \sum_\alpha \bar{\eta}^{(\alpha)}$,	entropy density per unit reference volume;
$\vartheta > 0$,	absolute temperature;
$\nabla\vartheta$,	referential temperature gradient;
$\mathbf{q}_{\mathrm{R}}$,	referential heat flux vector;
q_{R},	scalar heat supply.

In order to account for the major strain-hardening and softening characteristics of polymeric materials observed during viscoplastic deformation, we introduce macroscopic *internal variables* to represent important aspects of the microstructural resistance to plastic flow. Specifically, we introduce[5]

- A list of m scalar *internal state-variables*

$$\boldsymbol{\xi}^{(\alpha)} = (\xi_1^{(\alpha)}, \xi_2^{(\alpha)}, \ldots, \xi_m^{(\alpha)})$$

  for each α.

Further,

- we limit our attention to situations under which the material may be idealized to be *isotropic*. Accordingly, all constitutive functions are presumed to be isotropic in character.

3.1 Constitutive equations

1. **Free energy:**

   We assume that the free energy has the separable form

$$\psi_{\mathrm{R}} = \sum_\alpha \bar{\psi}^{(\alpha)}(\mathcal{I}_{\mathbf{C}^{e\,(\alpha)}}, \vartheta), \tag{3.5}$$

   where $\mathcal{I}_{\mathbf{C}^{e\,(\alpha)}}$ represents a list of the principal invariants of $\mathbf{C}^{e\,(\alpha)}$.

[5] In Srivastava et al. (2009) we had also included a list of *symmetric and unimodular* tensor fields

$$\mathbf{A}^{(\alpha)}(\mathbf{X}, t), \quad \mathbf{A}^{(\alpha)} = \mathbf{A}^{(\alpha)\top}, \quad \det\mathbf{A}^{(\alpha)} = 1,$$

as additional internal variables. Each such tensor field represents a dimensionless *squared stretch-like* quantity, which as a linear transformation, maps vectors in the intermediate structural space for each α, into vectors in the same space. Such a list of internal variables was included in our previous paper to allow for modeling cyclic-loading and Bauschinger-like phenomena in polymers. Here, since we do not have any experimental data on cyclic loading for the tBA/PEGDMA shape-memory polymer, we consider a simpler theory which does not include such internal variables.

2. **Cauchy stress:**

The Cauchy stress in the deformed body is the sum of the contributions from each micromechanism

$$\mathbf{T} = \sum_{\alpha} \mathbf{T}^{(\alpha)}, \tag{3.6}$$

with

$$\mathbf{T}^{(\alpha)} \stackrel{\text{def}}{=} J^{-1} \left(\mathbf{F}^{e\,(\alpha)} \mathbf{S}^{e\,(\alpha)} \mathbf{F}^{e\,(\alpha)\top} \right), \qquad \mathbf{T}^{(\alpha)} = \mathbf{T}^{(\alpha)\top}, \tag{3.7}$$

where

$$\mathbf{S}^{e\,(\alpha)} = 2\, \frac{\partial \bar{\psi}^{e\,(\alpha)}(\mathcal{I}_{\mathbf{C}^{e\,(\alpha)}}, \vartheta)}{\partial \mathbf{C}^{e\,(\alpha)}} \tag{3.8}$$

is a symmetric second Piola stress defined with respect to the local intermediate structural space for each α.

The driving stress for plastic flow is the *symmetric* Mandel stress

$$\mathbf{M}^{e\,(\alpha)} = \mathbf{C}^{e\,(\alpha)} \mathbf{S}^{e\,(\alpha)}. \tag{3.9}$$

Correspondingly, the scalar

$$\bar{\tau}^{(\alpha)} \stackrel{\text{def}}{=} \frac{1}{\sqrt{2}} \, |\mathbf{M}_0^{e\,(\alpha)}| \tag{3.10}$$

defines an *equivalent shear stress* for each α.

3. **Flow rules:**

The evolution equation for each $\mathbf{F}^{p\,(\alpha)}$, with $\mathbf{W}^{p\,(\alpha)} = \mathbf{0}$,[6] is

$$\dot{\mathbf{F}}^{p\,(\alpha)} = \mathbf{D}^{p\,(\alpha)}\, \mathbf{F}^{p\,(\alpha)}, \tag{3.11}$$

with the plastic stretching given by

$$\mathbf{D}^{p\,(\alpha)} = \nu^{p\,(\alpha)} \left(\frac{\mathbf{M}_0^{e\,(\alpha)}}{2\, \bar{\tau}^{(\alpha)}} \right), \tag{3.12}$$

where

$$\nu^{p\,(\alpha)} \stackrel{\text{def}}{=} \sqrt{2}\, |\mathbf{D}^{p\,(\alpha)}|\,, \tag{3.13}$$

is an *equivalent plastic shear strain rate*.

Let

$$\mathbf{\Lambda}^{(\alpha)} = (\mathbf{C}^{e\,(\alpha)}, \mathbf{B}^{p\,(\alpha)}, \boldsymbol{\xi}^{(\alpha)}, \vartheta) \tag{3.14}$$

denote a list of constitutive variables. Then, for given $\bar{\tau}^{(\alpha)}$ and $\mathbf{\Lambda}^{(\alpha)}$, the equivalent plastic shear strain rate $\nu^{p\,(\alpha)}$ is obtained by solving a scalar strength relation

$$\bar{\tau}^{(\alpha)} = Y^{(\alpha)}(\mathbf{\Lambda}^{(\alpha)}, \nu^{p\,(\alpha)}), \tag{3.15}$$

where the strength function $Y^{(\alpha)}(\mathbf{\Lambda}^{(\alpha)}, \nu^{p\,(\alpha)})$ is an isotropic function of its arguments.

4. **Evolution equations for internal variables:**

The internal variables $\boldsymbol{\xi}^{(\alpha)}$ are presumed to evolve according to the differential equations

$$\dot{\xi}_i^{(\alpha)} = \underbrace{h_i^{(\alpha)}(\mathbf{\Lambda}^{(\alpha)})\, \nu^{p\,(\alpha)}}_{\text{dynamic evolution}} - \underbrace{\mathcal{R}_i^{(\alpha)}(\mathbf{\Lambda}^{(\alpha)})}_{\text{static recovery}}, \tag{3.16}$$

with the functions $h_i^{(\alpha)}$ and $\mathcal{R}_i^{(\alpha)}$ isotropic functions of their arguments.

[6] For a detailed discussion and justification of the $\mathbf{W}^p = \mathbf{0}$ assumption in a single micro-mechanism isotropic theory, see Gurtin and Anand (2005). On purely pragmatic grounds we adopt such an assumption here as well.

The evolution equations for $\mathbf{F}^{p\,(\alpha)}$ and $\boldsymbol{\xi}^{(\alpha)}$ need to be accompanied by initial conditions. Typical initial conditions presume that the body is initially (at time $t = 0$, say) in a **virgin state** in the sense that

$$\mathbf{F}(\mathbf{X}, 0) = \mathbf{F}^{p\,(\alpha)}(\mathbf{X}, 0) = \mathbf{1}, \qquad \xi_i^{(\alpha)}(\mathbf{X}, 0) = \xi_{i,\,0}^{(\alpha)} \ (= \text{constant}), \tag{3.17}$$

so that by $\mathbf{F} = \mathbf{F}^{e\,(\alpha)}\mathbf{F}^{p\,(\alpha)}$ we also have $\mathbf{F}^{e\,(\alpha)}(\mathbf{X}, 0) = \mathbf{1}$.

5. **Entropy relation:**

   The entropy relation is given by

$$\eta_{\mathrm{R}} = \sum_{\alpha} \eta^{(\alpha)}, \qquad \eta^{(\alpha)} = -\frac{\partial \bar{\psi}^{e\,(\alpha)}(\mathcal{I}_{\mathbf{C}^{e\,(\alpha)}}, \vartheta)}{\partial \vartheta}. \tag{3.18}$$

6. **Fourier's Law:**

   To the constitutive equations listed above, we append a simple Fourier's law for the heat flux

$$\mathbf{q}_{\mathrm{R}} = -\kappa\, \nabla \vartheta, \tag{3.19}$$

   with $\kappa(\vartheta) > 0$ the thermal conductivity.

3.2 Partial differential equations for the deformation and temperature fields

The partial differential equation for the deformation is obtained from the local force balance

$$\mathrm{Div}\, \mathbf{T}_{\mathrm{R}} + \mathbf{b}_{0\mathrm{R}} = \rho_{\mathrm{R}}\, \ddot{\boldsymbol{\chi}}, \tag{3.20}$$

where $\mathbf{b}_{0\mathrm{R}}$ is the non-inertial body force per unit volume of the reference body, $\rho_{\mathrm{R}} > 0$ is the mass density, and

$$\mathbf{T}_{\mathrm{R}} = J\mathbf{T}\mathbf{F}^{-\top} \tag{3.21}$$

is the standard first Piola stress, with $\mathbf{T}$ given by (3.6) through (3.8).

The specific heat in the theory is given by

$$c \stackrel{\text{def}}{=} -\vartheta \sum_{\alpha} \frac{\partial^2 \bar{\psi}^{e\,(\alpha)}(\mathcal{I}_{\mathbf{C}^{e\,(\alpha)}}, \vartheta)}{\partial \vartheta^2}\,, \tag{3.22}$$

and balance of energy gives the following partial differential equation for the temperature

$$c\dot{\vartheta} = -\mathrm{Div}\, \mathbf{q}_{\mathrm{R}} + q_{\mathrm{R}} + \sum_{\alpha}\ \bar{\tau}^{(\alpha)}\, \nu^{p\,(\alpha)} + \underbrace{\vartheta \sum_{\alpha} \frac{\partial^2 \bar{\psi}^{e(\alpha)}}{\partial \vartheta\, \partial \mathbf{C}^{e\,(\alpha)}} : \dot{\mathbf{C}}^{e\,(\alpha)}}_{\text{“thermoelastic” coupling term}}, \tag{3.23}$$

with $\mathbf{q}_{\mathrm{R}}$ given by (3.19). The thermo-elastic coupling terms which appear in (3.23), are a standard consequence of continuum thermodynamics; specifically, the term

$$\frac{\partial^2 \bar{\psi}^{e(\alpha)}}{\partial \vartheta\, \partial \mathbf{C}^{e\,(\alpha)}} = \frac{\partial}{\partial \vartheta} \left(\frac{\partial \bar{\psi}^{e(\alpha)}}{\partial \mathbf{C}^{e\,(\alpha)}} \right)$$

represents the variation of stress with temperature, a quantity which may be referred to as a *stress-temperature modulus* for the αth micromechanism, and $\dot{\mathbf{C}}^{e(\alpha)}$ represents a corresponding elastic "strain rate."

The specialization of the theory for application to *thermoset* shape-memory amorphous polymers is described in the Appendix. As discussed there, we limit our attention to a theory with three "micromechanisms" ($M = 3$). The material parameters appearing in the specialized theory were calibrated by fitting the experimental stress-strain data for tBA/PEGDMA shown in Fig. 1, by following a procedure

described in detail in Srivastava et al. (2009); these material parameters are listed in Table 1. The stress-strain curves calculated using the specialized model and the material parameters for tBA/PEGDMA are plotted in Fig. 1 as dashed lines. As shown in this figure, the constitutive model reasonably accurately reproduces all the major features of the macroscopic stress-strain response of the material both in the "glassy-polymer" regime below ϑ_g and the "hysteretic-rubber" response above ϑ_g.

REMARK 2. Theories of the type considered here, even in the linear-viscoelasticity regime, typically require a large number of Maxwell-elements M, with an associated large number of spring-constants and dashpot-viscosities to fit experimentally observed stress-relaxation, creep and other mechanical response characteristics of polymers in the small strain regime. In the large-deformation theory considered here, our goal was to choose the minimum number of micro-mechanisms M, and thereby the associated number of material parameters, which can replicate the experimentally-observed stress-strain curves in the strain, strain-rate, and temperature range of interest with reasonable accuracy. Nevertheless, the number of material parameters for tBA/PEGDMA listed in Table 1 is still quite large. This is a limitation of this class of phenomenological continuum-level theories. However, once the material parameters are calibrated, as we show next, the theory is able to predict the response of the material in complex three-dimensional geometries which are subjected to a variety of thermo-mechanical histories.

REMARK 3. We have numerically implemented the theory by writing a user-material subroutine for a widely-used finite element program ABAQUS/Standard (2009). For brevity, we do not give the details of this numerical implementation in this paper.

4 Validation experiments and simulations

In order to validate the predictive capabilities of our constitutive theory and its numerical implementation, in this section we show the results of two thermo-mechanical experiments that we have performed on the tBA/PEGDMA shape-memory polymer, and compare the results of macroscopic measurements from these experiments against results from corresponding numerical simulations. The validation experiments considered below are

(i) Measurement of the *force-versus-time* response of a ring-shaped specimen of tBA/PEGDMA which was subjected to the following thermo-mechanical history: the specimen was heated to a temperature above ϑ_g of the material, the ring was then compressed into an oval shape, the compression grips were then held *fixed* while the specimen was first cooled to a temperature below ϑ_g, and then heated back to its initial temperature above ϑ_g. We call an experiment of this type a *constrained-recovery* experiment.

(ii) Measurement of the *displacement-versus-time* response of a planar specimen of tBA/PEGDMA in the shape of a diamond-shaped lattice which was subjected to the following thermo-mechanical history: the specimen was compressed between two platens at temperature above ϑ_g of the material, the compression platens were then held *fixed* while the specimen was cooled to a temperature below ϑ_g. The constraint of the platens was then removed, and the specimen was heated to a temperature above ϑ_g and allowed to freely recover its shape. We call an experiment of this type an *unconstrained-recovery* or a *free-recovery* experiment.

Both thermo-mechanical experiments were conducted on an EnduraTEC Electroforce 3200 testing machine equipped with a furnace. The temperature of the polymer was measured by using a thermo-couple attached to the specimen. In the numerical simulations we prescribed the measured temperature profile to all nodes in the finite element mesh, and *neglected* transient heat conduction within the polymer since these effects were quite small.

Finally, as a demonstration of the robustness of our three-dimensional numerical simulation capability, we also show results from a simulation of the shape-recovery response of a stent made from the polymer when it is inserted in an artery modeled as a compliant elastomeric tube.

4.1 Force-time response of a ring-shaped specimen subjected to a constrained-recovery experiment

The flat specimen, 3 mm thick, was ring-shaped with two extension arms which were used for gripping the specimen. The ring portion of the specimen had an outer diameter of 11.9 mm and an inner diameter of 6.3 mm, while the extension arms were each 12.7 mm long and 4.1 mm wide. The experimental set-up with the tBA/PEGDMA specimen mounted in place within the furnace of the EnduraTEC testing machine is shown in Fig. 2. The top and the bottom flat surfaces of the extension arms were rested against the base of the grips, and the vertical sides were securely tightened in the grips.

The specimen was subjected to the following thermo-mechanical history: (i) it was heated to 58 C and gripped; (ii) the bottom grip was fixed in place while the top grip was moved downwards at a velocity 0.01 mm s^{-1} for a total displacement of 2.5 mm to deform the ring; (iii) the grips were then held fixed in their positions and the specimen was first cooled to 32 C and then heated back to 58 C. The displacement and temperature histories for the experiment are shown in Fig. 3a. The reaction forces during the experiment were recorded using a load-cell, and the measured force-versus-time curve is shown in Fig. 3b.

For the finite element simulation of this constrained-recovery experiment we make use of the symmetry of the geometry, and only mesh one-eighth of the geometry using 537 ABAQUS-C3D8HT thermo-mechanically-coupled elements; Fig. 4a. Referring to this figure, all the nodes on the surface formed by CD extending into the 3-direction were prescribed displacement boundary conditions which enforced symmetry in the 1-direction, all the nodes on the surface formed by AB extending into the 3-direction were prescribed symmetry in the 2-direction, and all the nodes on the front surface defined by ABCD were prescribed symmetry in the 3-direction. A displacement history was prescribed to the highlighted nodes on the outer surface of the extension arm such that the displacement history for the complete geometry matched that of the experiment. The experimentally-measured temperature history was prescribed to the whole mesh. Fig. 4b shows the deformed mesh at the end of the compression step.

Fig. 3b compares the experimentally-measured and the numerically-predicted force-versus-time curves. The measurements from the experiment show that a compressive force was generated during the deformation at 58 C. Subsequently, under the fixed-grip conditions, upon cooling to 32 C the compressive force gradually reduces and transitions to a state of tension; and finally, upon heating back to 58 C, the reaction force transitions back to a compressive state. As shown in Fig. 3b, the simulation is able to reasonably accurately predict the force-versus-time response for the constrained-recovery experiment.

4.2 Displacement-time response of a diamond-lattice-shaped specimen subjected to an unconstrained-recovery experiment

The flat diamond-lattice-shaped specimen, Fig. 5a, was 50 mm wide, 35 mm tall, and 3 mm thick. Each diamond-shaped cut-out was a square with 6.5 mm sides with a 1 mm fillet-radius at the corners; the width of the ligaments forming the lattice was 2.16 mm.

The specimen was subjected to the following thermo-mechanical history: (i) it was compressed between two platens at 60 C at a relative platen velocity of 0.02 mm s^{-1}, and the height of the specimen was reduced from 35 mm to 20.5 mm — this resulted in an increase in its width from 50 mm to 59.5 mm; (ii) the platens were held in place and the specimen was cooled to 21 C following a temperature profile similar to what is shown in Fig. 3a — the deformed shape is shown in Fig. 5b; (iii) the compression platens were then removed and the specimen was heated to 58 C according to the temperature-versus-time history shown in Fig. 6. The dimensional changes in the specimen during this unconstrained-recovery phase were measured using a video-extensometer. The experimentally-measured stretches (L/L_0) in the 1- and 2-directions as functions of temperature and time during the unconstrained heating phase of the experiment are shown in Fig. 7 and Fig. 8, respectively.

For the finite element simulation of this experiment we make use of the symmetry of the geometry and only mesh one-eighth of the geometry, using 1962 ABAQUS-C3D8HT thermo-mechanically-coupled elements, Fig. 9. Referring to this figure, all the nodes on the 2-3 symmetry plane were prescribed symmetry displacement boundary conditions in the 1-direction, all the nodes on the 1-3 symmetry plane were prescribed symmetry boundary conditions in the 2-direction, and all the nodes on the front surface were prescribed symmetry boundary conditions in the 3-direction. The displacement history was prescribed

to the highlighted nodes on the top surface during the hot-deformation and cooling steps. Our numerical simulation included all the steps described above for the thermo-mechanical history, including the initial hot-deformation, cooling, and finally the unconstrained shape-recovery with the applied temperature change. The results from the numerical simulation for the stretch in the 2-direction versus the temperature for the complete thermo-mechanical cycle are shown in Fig. 10. Fig. 7 and Fig. 8 compare the numerically-predicted and experimentally-measured stretches in the 1- and 2-directions versus temperature and time, respectively, during the unconstrained heating phase of the experiment. The numerically-predicted results are in good agreement with experimental measurements.

Finally, the left pane in Fig. 11 shows images of the specimen at various temperatures during unconstrained shape-recovery, while the right pane in this figure shows corresponding predictions from the numerical simulations.[7] The shapes at various temperatures predicted by the numerical simulation closely match those which were observed in the experiment.

4.3 Numerical simulation of insertion of a stent in an artery

Shape-memory polymers have been proposed as potential materials for stents which expand and/or support blood vessels, and several experimental demonstrations of this concept have been published in the literature (e.g., Wache et al., 2003; Yakacki et al., 2007; Baer et al., 2007b). However, to the best of our knowledge, no reports of a numerical-simulation capability that can aid in understanding the performance of shape-memory-polymer-based stents exist in the current literature. As a demonstration of the robustness of our three-dimensional numerical-simulation capability in what follows we show results from a simulation of the shape-recovery response of a stent made from tBA/PEGDMA when it is inserted in an artery, with the latter modeled as a tube made from a nonlinear elastic material. Note that this is purely a numerical exercise to show the robustness of the constitutive theory and its implementation, we have not attempted to reproduce the actual deployment of a stent in a human body.

In our simulation we considered a cylindrical stent made from tBA/PEGDMA with diamond-shaped perforations, similar to those in the planar geometry considered in the previous subsection. The stent was modeled to have an initial length of 8 mm, and the outer and inner diameters of the stent were modeled as 8 mm and 7 mm, respectively. For the artery, we assumed a tubular geometry with an inner diameter of 5 mm, a wall thickness of 0.35 mm, and a length of 50 mm. The artery was modeled as an incompressible elastic Neo-Hookean material with a shear modulus of 33.33 kPa.

The stent was subjected to the following thermo-mechanical history: (i) it was radially compressed above ϑ_g at 60 C to reduce its outer diameter to 4.7 mm; (ii) cooled under kinematical constraints to 22 C at a rate of 0.1 C s^{-1} to fix its deformed shape; (iii) the constraints were removed; (iv) following which it was inserted into an arterial tube; and (v) was heated back to 60 C at a rate of 0.1 C s^{-1} to allow the stent to attempt to recover its initial shape under the constraints imposed by the artery.[8]

Due to the symmetry of the problem in our simulation we considered only one-eighth of the stent geometry, which was modeled using 1077 ABAQUS-C3D8HT thermo-mechanically-coupled elements, Fig. 12. The displacement boundary conditions prescribed to the stent were as follows: symmetry in the 1-direction for all the nodes on the surface defined by edge CD extending into the 3-direction; symmetry in the 2-direction for all the nodes on the surface defined by edge AB extending into the 3-direction; and symmetry in the 3-direction for all the highlighted nodes on the front surface. To apply the initial deformation above ϑ_g, all of the nodes at the outer diameter were given an inward radial displacement.

The finite element mesh for the artery consisted of 1500 ABAQUS-C3D8H elements: 2 elements through the thickness, 50 elements along the length, and 15 elements around the one-quarter circumference. For the artery, the displacement boundary conditions $u_1 = 0$, $u_2 = 0$ and $u_3 = 0$ were applied for all the nodes on the face perpendicular to the 3-direction and away from the stent; symmetry in the 3-direction was applied to all the nodes that were on the face perpendicular to the 3-direction and close to the stent. Contact between the stent and artery was modeled as frictionless.

Predictions from the numerical simulation for the outer-diameter of the stent at different temperatures during the imposed thermo-mechanical history of insertion of a stent in an artery are shown in Fig. 13. These

[7] In Fig. 11, for ease of visualization, we have mirrored the simulation results along the symmetry planes.

[8] We emphasize that this a purely numerical exercise; no actual stent for application in humans is expected to be heated to 60 C!

simulation results show that the outer diameter of the stent recovered from 4.74 mm to 6.06 mm by the time the temperature reached 47 C during heating; further heating to 60 C only increased the outer diameter from 6.06 mm to 6.22 mm; that is, 90% of the total shape-recovery occurred by the time the stent was heated to 47 C. Fig. 14a shows the initial undeformed stent, while Fig. 14b shows the deformed stent after radial compression at 60 C. Fig. 14c shows snapshots of the stent inside the artery during shape-recovery at 22 C, 42 C, and 60 C.

5 Concluding remarks

We have developed a thermo-mechanically-coupled large-deformation constitutive theory and a numerical simulation capability for modeling the response of thermally-actuated shape-memory polymers. The theory and methodology developed in this study offers the potential for the development of a robust simulation-based capability for the design of devices made from shape-memory polymers for a variety of applications. Such a capability should help reduce the amount of expensive experimentation.

In closing, we would like to point out some limitations of the present theory and its implementation, which need additional future work:

- In the specialization of the theory for the applications considered here (cf. Section 6, Appendix), we have neglected the static recovery terms in the evolution equations for the internal variables (cf. (3.16)). It is clear that this is not a suitable approximation for arbitrary thermo-mechanical histories, especially if the initial deformation of the material is performed below ϑ_g, rather than above ϑ_g.

- The fit of the specialized constitutive model to the experimental data in the *vicinity* of the *rate-dependent* ϑ_g (cf. Figure 1) is not optimal. Additionally, in the vicinity of ϑ_g our constitutive equations are quite stiff; hence, care needs to be exercised in developing robust numerical time-integration schemes which take suitable-sized time-steps in this regime.

- With reference to Figures 3b and 8, the predicted force-time and the stretch-time recovery responses are faster than the corresponding experimental results; at the present time we do not fully understand the cause of this discrepancy.

Acknowledgements

This work was supported by the National Science Foundation under grant number DMI-0517966, and the MST program of the Singapore-MIT Alliance. We are grateful to Mr. Claudio Di Leo of our laboratory for his help in fabricating shape-memory polymer specimens.

References

Abaqus/Standard, 2009. SIMULIA, Providence, RI.

Ames, N. M., Srivastava, V., Chester, S. A., and Anand, L., 2009. A thermo-mechanically-coupled theory for large deformations of amorphous polymers. Part II: applications. *International Journal of Plasticity* 25, 1495-1539.

Anand, L., 1979. On H. Hencky's approximate strain-energy function for moderate deformations. *ASME Journal of Applied Mechanics* 46, 78-82.

Anand, L., 1986. Moderate deformations in extension-torsion of incompressible isotropic elastic materials. *Journal of the Mechanics and Physics of Solids* 34, 293-304.

Anand, L., and Gurtin, M. E., 2003. A theory of amorphous solids undergoing large deformations, with applications to polymeric glasses. *International Journal of Solids and Structures* 40, 1465-1487.

Anand, L., and Ames, N. M., 2006. On modeling the micro-indentation response of an amorphous polymer. *International Journal of Plasticity* 22, 1123-1170.

Anand, L., Ames, N. M., Srivastava, V., and Chester, S. A., 2009. A thermo-mechanically-coupled theory for large deformations of amorphous polymers. Part I: formulation. *International Journal Plasticity* 25, 1474-1494.

Arruda, E. M., and Boyce, M. C., 1993. A three-dimensional constitutive model for the large stretch behavior of rubber elastic materials. *Journal of the Mechanics and Physics of Solids* 41, 389-412.

Baer, G. M., Wilson, T. S., Matthews, D. L., and Maitland, D. J., 2007. Shape memory behavior of thermally stimulated polyurethane for medical applications. *Journal of Applied Polymer Science* 103, 3882-3892.

Baer, G. M., Small, W., Wilson, T. S., Benett, W. J., Matthews, D. L., Hartman, J., and Maitland, D. J., 2007. Fabrication and in vitro deployment of a laser-activated shape-memory vascular stent. *Biomedical Engineering Online* 6.

Behl, M., and Lendlein, A., 2007. Shape memory polymers. *Materials Today* 10, 20-28.

Bergstrom J. S., and Boyce, M. C., 1988. Constitutive modeling of the large strain time-dependent behavior of elastomers. *Journal of the Mechanics and Physics of Solids* 46, 931-954.

Boyce, M. C., Parks, D. M., and Argon, A. S., 1988. Large inelastic deformation of glassy polymers. Part 1: rate dependent constitutive model. *Mechanics of Materials* 7, 15-33.

Boyce, M. C., 1996. Direct comparison of the Gent and the Arruda-Boyce constitutive models of rubber elasticity. *Rubber Chemistry and Technology* 69, 781-785.

Boyce, M. C., Socrate, S., and Llana, P. G., 2000. Constitutive model for the finite deformation stressstrain behavior of poly(ethylene terephthalate) above the glass transition. *Polymer* 41, 2183-2201.

Buckley, C. P., and Jones, D. C., 1995. Glass-rubber constitutive model for amorphous polymers near the glass transition. *Polymer* 36, 3301-3312.

Campbell, D., Lake, M. S., Scherbarth, M. R., Nelson, E., and Six, R. W., April 2005. Elastic memory composite material: an enabling technology for future furlable space structures. In *46th AIAA/ASME/ASCE/AHS/ASC Structures, Structural Dynamics and Materials Conference*, Austin, Texas.

Chen, Y. C., and Lagoudas, D. C., 2008. A constitutive theory for shape-memory polymers. Part I Large deformations. *Journal of the Mechanics and Physics of Solids* 56, 1752-1765.

Dooling, P. J., Buckley, C. P., Rostami, S., and Zahalan, N., 2002. Hot-drawing of poly(methyl methacrylate) and simulation using a glass-rubber consitutive model. *Polymer* 43, 2451-2465.

Dupaix, R. B. and Boyce, M. C., 2007. Constitutive modeling of the finite strain behavior of amorphous polymers in and above the glass transition. *Mechanics of Materials* 39, 39-52.

Fulcher, G. S., 1925. Analysis of recent measurements of the viscosity of glasses. *Journal of the American Ceramic Society* 8, 339-355.

Gall, K., Kreiner, P., Turner, D., and Hulse, M., 2004. Shape memory polymers for microelectromechanical systems. *Journal of Microelctromechanical Systems* 13, 472-483.

Gall, K., Yakacki, C. M., Liu Y., Shandas, R., Willett, N., and Anseth, K. S., 2005. Thermomechanics of the shape-memory effect in polymers for biomedical applications. *Journal of Biomedical Materials Research Part A* 73A, 339-348.

Gent, A. N., 1996. A new constitutive relation for rubber. *Rubber Chemistry and Technology* 69, 59-61.

Govaert, L. E., Timmermans, P. H. M., and Brekelmans, W. A. M., 2000. The influence of intrinsic strain softening on strain localization in polycarbonate: modeling and experimental validation. *Journal of Engineering Materials and Technology* 122, 177-185.

Gurtin, M. E., Fried, E., and Anand, L., 2009. *The Mechanics and Thermodynamics of Continua*, Cambridge University Press, New York (forthcoming).

Gurtin, M. E., and Anand, L., 2005. The decomposition $\mathbf{F} = \mathbf{F}^e\mathbf{F}^p$, material symmetry, and plastic irrotationality for solids that are isotropic-viscoplastic or amorphous. *International Journal of Plasticity* 21, 1686-1719.

Jiang, H. Y., Kelch, S., and Lendlein, A., 2006. Polymers move in response to light. *Advanced Materials* 18, 1471-1475.

Kröner, E., 1960. Allgemeine kontinuumstheorie der versetzungen und eigenspannungen. *Archive for Rational Mechanics and Analysis* 4, 273-334.

Lee, E. H., 1969. Elastic plastic deformation at finite strain. *ASME Journal of Applied Mechanics* 36, 1-6.

Lendlein, A., and Langer, R., 2002. Biodegradable, elastic shape-memory polymers for potential biomedical applications. *Science* 296, 1673-1676.

Lendlein, A., Jiang, H., Jünger, O., and Langer, R., 2005. Light-induced shape-memory polymers. *Nature* 434, 879-882.

Liu, Y., Gall, K., Dunn, M. L., Greenberg, A. R., and Diani, J., 2006. Thermomechanics of shape-memory polymers: Uniaxial experiments and constitutive modeling. *International Journal of Plasticity* 22, 279-313.

Maitland, D. J., Metzger, M. F., Schumann, D., Lee, A., and Wilson, T. S., 2002. Photothermal properties of shape-memory polymer micro-actuators for treating stroke. *Lasers in Surgery and Medicine* 30, 1-11.

Metcalfe, A., Desfaits, A., and Salazkin, I., 2003. Cold hibernated elastic memory foams for endovascular interventions. *Biomaterials* 24, 491-497.

Metzger, M. F., Wilson, T. S., Schumann, D., Matthews, D. L., and Maitland, D. J., 2002. Mechanical properties of mechanical actuator for treating ischemic stroke. *Biomedical Microdevices* 4, 89-96.

Nguyen, T. D., Qi, H. J., Castro, F., and Long, K. N., 2008. A thermoviscoelastic model for amorphous shape-memory polymers: Incorporating structural and stress relaxation. *Journal of the Mechanics and Physics of Solids* 56, 2792-2814.

Ota, S., 1981. A current status of irradiated heat-shrinkable tubing in Japan. *Radiation Physics and Chemistry* 18, 81-87.

Parks, D. M., Argon, A. S., and Bagepalli, B., 1985. Large elastic-plastic deformation of glassy polymers. Part 1: Constitutive modelling. Report, MIT, Program in Polymer Science and Technology.

Qi, H. J., Nguyen, T. D., Castro, F., Yakacki, C. M., and Shandas, R., 2008. Finite deformation thermomechanical behavior of thermally induced shape-memory polymers. *Journal of the Mechhanics and Physics of Solids* 56, 1730-1751.

Ratna, D., and Kocsis, J. K., 2008. Recent advances in shape-memory polymers and composites: a review. *Journal of Materials Science* 43, 254-269.

Richeton, J., Ahzi, S., Vecchio, K. S., Jiang, F. C., and Makardi, A., 2007. Modeling and validation of the large deformation inelastic response of amorphous polymers over a wide range of temperatures and strain rates. *International Journal of Solids and Structures* 44, 7938-7954.

Safranski, D., and Gall, K., 2008. Effect of chemical structure and crosslinking density on the thermomechanical properties and toughness of (meth)acrylate shape-memory polymer networks. *Polymer* 49, 4446-4455.

Srivastava, V., Chester, S. A., Ames, N. M., and Anand, L., 2010. A thermo-mechanically-coupled large-deformation theory for amorphous polymers in a temperature range which spans their glass transition. *International Journal of Plasticity*, doi:10.1016/j.ijplas.2010.01.004.

Tammann, V. G., and Hesse, W., 1926. Die abhängigkeit der viscosität von der temperatur bei unterkühlten flüssigkeiten. *Zeitschrift für anorganische und allgemeine Chemie* 156, 245-257.

Tobushi, H., Hara, H., Yamada, E., and Hayashi, S., 1996. Thermomechanical properties in a thin film of shape-memory polymer of polyurethane series. *Smart Materials and Structures* 5, 483-491.

Vettiger, P., Cross, G., Despont, M., Drechsler, U., Dürig, U., Gotsmann, B., Häberle, W., Lantz, M. A., Rothuizen, H. E., Stutz, R., and Binning, G. K., 2002. The "Millipede"—nanotechnology entering data storage. *IEEE Transactions on Nanotechnology* 1, 39-55.

Vogel, H., 1921. Das temperaturabhängigkeitsgesetz der viskosität von flüssigkeiten. *Physikalische Zeitschrift* 22, 645-646.

Wache, H. M., Tartakowska, D. J., Hentrich, A., and Wagner, M. H., 2003. Development of a polymer stent with shape-memory effect as a drug delivery system. *Journal of Materials Science: Materials in Medicine* 14, 109-112.

Williams, M. L., Landel, R. F., and Ferry, J. D., 1955. The temperature dependence of relaxation mechanisms in amorphous polymers and other glass-forming liquids. *Journal of the American Chemical Society* 77, 3701-3707.

Wornyo, E., Gall, K., Yang, F., and King, W., 2007. Nanoindention of shape-memory polymer networks. *Polymer* 48, 3213-3225.

Yakacki, C. M., Shandas, R., Lanning, C., Rech, B., Eckstein, A., and Gall, K., 2007. Unconstrained recovery characterization of shape-memory polymer networks for cardiovascular applications. *Biomaterials* 28, 2255-2263.

6 Appendix

Here, we specialize the constitutive theory discussed in §3 for application to amorphous thermoset shape-memory polymers in the strain, strain-rate, and temperature range of interest shown in Fig. 1. Based on our previous experience with modeling the response of amorphous thermoplastic polymers (Srivastava et al., 2009), we consider a theory with three micromechanisms, $M = 3$. Although no real material is composed of springs and dashpots, as a visual aid, Fig. 15 shows a schematic "spring-dashpot" rheological representation of our three micromechanism model. These three micromechanisms are intended to represent the following underlying physical phenomena:

- **The first micromechanism ($\alpha = 1$)**: The nonlinear spring represents an "elastic" resistance due to intermolecular energetic bond-stretching. The dashpot represents thermally-activated plastic flow due to "inelastic mechanisms," such as chain-segment rotation and relative slippage of the polymer chains between neighboring cross-linkage points.

- **The second and third micromechanisms ($\alpha = 2, 3$)**: In addition to the chemical crosslinks which are present throughout the temperature range of interest in thermoset polymers, at temperatures below ϑ_g we expect that the polymer also exhibits a significant amount of mechanical-crosslinking. We conceptually distinguish molecular chains between mechanical-crosslinks and molecular chains between chemical-crosslinks by introducing two micromechanisms $\alpha = 2$ and $\alpha = 3$, respectively. The nonlinear springs in these two mechanisms represent resistances due to changes in the free energy upon stretching of the molecular chains between the crosslinks. The mechanical-crosslinks are expected to disintegrate when the temperature is increased through ϑ_g; the dashpot in micromechanism $\alpha = 2$ represents thermally-activated plastic flow resulting from such a phenomenon. The micromechanism $\alpha = 3$

represents chemically-crosslinked backbone of the thermoset polymer in which the crosslinks do not slip; accordingly we do not use a dashpot for this micromechanism, and we set $\mathbf{F}^{p(3)} = \mathbf{1}$, so that $\mathbf{F}^{e(3)} = \mathbf{F}$.

Our strategy to phenomenologically model the response of the material as the temperature traverses ϑ_g is as follows:

(i) For temperatures $\vartheta < \vartheta_g$, we do not allow any plastic flow in the dashpot associated with micromechanism $\alpha = 2$. Thus, since the springs in $\alpha = 2$ and $\alpha = 3$ are in parallel, the three-micromechanism model reduces to a simpler two-micromechanism model, which we have recently successfully used to model the response of amorphous polymers for temperatures below ϑ_g (Anand et al., 2009; Ames et al., 2009).

(ii) For temperatures $\vartheta > \vartheta_g$, we allow for plastic flow in the dashpot associated with micromechanism $\alpha = 2$, but *quickly drop the plastic flow resistance in mechanism* $\alpha = 2$ *to a very small value*, so that for all practical purposes in this temperature range, only mechanisms $\alpha = 1$ and $\alpha = 3$ contribute to the macroscopic stress.

REMARK 4. As is well-known, the "glass transition" in amorphous polymers occurs over a narrow range of temperatures, and whatever the means that are used to define *a glass transition temperature* ϑ_g,[9] it also depends on the strain rate to which the material is subjected. With $\mathbf{D}_0 = \mathrm{sym}_0(\dot{\mathbf{F}}\mathbf{F}^{-1})$ denoting the total deviatoric stretching tensor, let

$$\nu \stackrel{\text{def}}{=} \sqrt{2}|\mathbf{D}_0| \tag{6.1}$$

denote an *equivalent shear strain rate*. As a simple model for the variation of the glass transition temperature with strain rate, we assume that

$$\vartheta_g = \begin{cases} \vartheta_r & \text{if} \quad \nu \leq \nu_r, \\ \vartheta_r + n \, \log\left(\dfrac{\nu}{\nu_r}\right) & \text{if} \quad \nu > \nu_r, \end{cases} \tag{6.2}$$

where ϑ_r a *reference glass transition temperature* at a *reference strain rate* ν_r, and n is a material parameter.

In the following subsections we present special constitutive equations for the three micromechanisms discussed above. For brevity we do not give a detailed development; the reader is referred to our recent papers (Anand et al., 2009; Ames et al., 2009; Srivastava et al., 2009) for the intermediate steps of continuum-mechanical arguments and derivations.

6.1 Constitutive equations for micromechanism $\alpha = 1$

1. **Free energy**

   Let

$$\mathbf{C}^{e(1)} = \sum_{i=1}^{3} (\lambda_i^e)^2 \, \mathbf{r}_i^e \otimes \mathbf{r}_i^e, \tag{6.3}$$

   denote the spectral representation of $\mathbf{C}^{e(1)}$, where $(\lambda_1^e, \lambda_2^e, \lambda_3^e)$ are the positive eigenvalues of $\mathbf{U}^{e(1)}$, and $(\mathbf{r}_1^e, \mathbf{r}_2^e, \mathbf{r}_3^e)$ are the orthonormal eigenvectors of $\mathbf{C}^{e(1)}$ and $\mathbf{U}^{e(1)}$. With

$$\mathbf{E}^{e(1)} = \sum_{i=1}^{3} E_i^e \, \mathbf{r}_i^e \otimes \mathbf{r}_i^e, \qquad E_i^e = \ln \lambda_i^e, \tag{6.4}$$

   denoting an elastic logarithmic strain measure, we consider an elastic free energy of the form[10]

$$\bar{\psi}^{(1)} = G|\mathbf{E}_0^{e\,(1)}|^2 + \tfrac{1}{2}K(\mathrm{tr}\,\mathbf{E}^{e(1)})^2 - 3\,K\,(\mathrm{tr}\,\mathbf{E}^{e(1)})\alpha^{\mathrm{th}}(\vartheta - \vartheta_0) + \tilde{f}(\vartheta), \tag{6.5}$$

[9] Such as the peak in the tan-δ curve in a DMA experiment.

[10] This is a useful free energy function for *moderately large elastic stretches*, Anand (1979, 1986).

where $\tilde{f}(\vartheta)$ is an entropic contribution to the free energy related to the temperature-dependent specific heat of the material. The temperature-dependent parameters

$$G(\vartheta) > 0, \quad K(\vartheta) > 0, \quad \alpha^{\rm th}(\vartheta) > 0, \tag{6.6}$$

are the shear modulus, bulk modulus, and coefficient of thermal expansion, respectively, and ϑ_0 is a reference temperature.

For polymeric materials the magnitude of the elastic shear modulus G decreases by a very significant amount as the temperature increases through the glass transition temperature of the material. Following Dupaix and Boyce (2007), we assume that the temperature dependence of the shear modulus may be approximated by the following function

$$G(\vartheta) = \tfrac{1}{2}(G_{gl} + G_r) - \tfrac{1}{2}(G_{gl} - G_r)\tanh\Big(\frac{1}{\Delta}(\vartheta - \vartheta_g)\Big) - M(\vartheta - \vartheta_g), \tag{6.7}$$

where ϑ_g is the glass transition temperature, G_{gl} and G_r ($< G_{gl}$) are values of the shear modulus in the glassy and rubbery regions, and Δ is a parameter related to the temperature range across which the glass transition occurs. The parameter M represents the slope of the temperature variation of G outside the transition region, with

$$M = \begin{cases} M_{gl} & \vartheta \le \vartheta_g, \\ M_r & \vartheta > \vartheta_g. \end{cases} \tag{6.8}$$

Next, the temperature dependence of Poisson's ratio $\nu^{\rm poi}$ of the material is assumed to be

$$\nu^{\rm poi}(\vartheta) = \frac{1}{2}(\nu^{\rm poi}_{gl} + \nu^{\rm poi}_r) - \frac{1}{2}(\nu^{\rm poi}_{gl} - \nu^{\rm poi}_r)\tanh\Big(\frac{1}{\Delta}(\vartheta - \vartheta_g)\Big), \tag{6.9}$$

with $\nu^{\rm poi}_{gl}$ and $\nu^{\rm poi}_r$ representing values below and above ϑ_g, respectively. The temperature dependence of the bulk modulus K is then obtained by using the standard relation for isotropic materials

$$K(\vartheta) = G(\vartheta) \times \frac{2(1 + \nu^{\rm poi}(\vartheta))}{3(1 - 2\,\nu^{\rm poi}(\vartheta))}. \tag{6.10}$$

The coefficient of thermal expansion is taken to have a bilinear temperature dependence, with the following contribution to the thermal expansion term $\alpha^{\rm th}(\vartheta - \vartheta_0)$ in the free energy relation (6.5):

$$\alpha^{\rm th}(\vartheta - \vartheta_0) = \begin{cases} \alpha_{gl}(\vartheta - \vartheta_0) & \text{if} \quad \vartheta \le \vartheta_g, \\ \alpha_{gl}(\vartheta - \vartheta_0) + (\alpha_r - \alpha_{gl})(\vartheta - \vartheta_g) & \text{if} \quad \vartheta > \vartheta_g. \end{cases} \tag{6.11}$$

2. **Cauchy stress. Mandel stress**

Corresponding to the special free energy (6.5), the contribution $\mathbf{T}^{(1)}$ to the Cauchy stress is given by

$$\mathbf{T}^{(1)} \stackrel{\rm def}{=} J^{-1}\,\mathbf{R}^{e\,(1)}\,\mathbf{M}^{e(1)}\,\mathbf{R}^{e\,(1)\top}, \tag{6.12}$$

where $\mathbf{M}^{e(1)}$, the Mandel stress, is given by

$$\mathbf{M}^{e(1)} = \frac{\partial\tilde{\psi}^{e\,(1)}(\mathbf{E}^{e(1)}, \vartheta)}{\partial\mathbf{E}^{e(1)}}, \tag{6.13}$$

which yields

$$\mathbf{M}^{e(1)} = 2G\mathbf{E}^{e\,(1)}_0 + K\,(\mathrm{tr}\,\mathbf{E}^{e(1)})\mathbf{1} - 3K\alpha^{\rm th}(\vartheta - \vartheta_0)\mathbf{1}; \tag{6.14}$$

note that $\mathbf{M}^{e(1)}$ is symmetric.

The Mandel stress is the driving stress for plastic flow in the theory. The corresponding *equivalent shear stress* and *mean normal pressure* are given by

$$\bar{\tau}^{(1)} \stackrel{\rm def}{=} \frac{1}{\sqrt{2}}\,|\mathbf{M}^{e\,(1)}_0|, \quad \text{and} \quad \bar{p} \stackrel{\rm def}{=} -\frac{1}{3}\mathrm{tr}\,\mathbf{M}^{e(1)}, \tag{6.15}$$

respectively.

3. **Internal variables**

For the micromechanism $\alpha = 1$, we restrict the list $\boldsymbol{\xi}^{(1)}$ of internal variables to three positive-valued scalars

$$\boldsymbol{\xi}^{(1)} = \Big(\varphi, S_a, S_b\Big),$$

where

- The parameters $\varphi \geq 0$ and $S_a \geq 0$ are introduced to model the "yield-peak" which is widely-observed in the intrinsic stress-strain response of glassy polymers. A key microstructural feature controlling the strain-softening associated with the "yield-peak" in glassy polymers is the local change in molecular-packing due to deformation-induced disordering. The variable φ, a positive-valued dimensionless "order"-parameter, is introduced to represent such *deformation-induced disordering*; and a stress-dimensioned internal variable S_a which is coupled to the microstructural disordering of the material, represents the corresponding *transient resistance* to plastic flow.
- The internal variable $S_b \geq 0$ represents a dissipative resistance to plastic flow to model "isotropic hardening" at large strains as the chains are pulled taut between entanglements resulting in increasing interaction between the neighboring chains and pendant side-groups; this is in addition to any entropic or energetic contribution from network chain-stretching.

4. **Flow rule**

The evolution equation for $\mathbf{F}^{p\,(1)}$ is

$$\dot{\mathbf{F}}^{p\,(1)} = \mathbf{D}^{p\,(1)}\,\mathbf{F}^{p\,(1)}, \tag{6.16}$$

with $\mathbf{D}^{p(1)}$ given by

$$\mathbf{D}^{p\,(1)} = \nu^{p\,(1)}\left(\frac{\mathbf{M}_0^{e\,(1)}}{2\bar{\tau}^{(1)}}\right). \tag{6.17}$$

Following our recent work on amorphous polymers (Srivastava et al., 2009, and references therein) we assume that the corresponding strength relation (3.15) at fixed $\boldsymbol{\Lambda}^{(1)}$ is invertible, and we choose a thermally-activated relation for the *equivalent plastic strain rate* in the specific form

$$\nu^{p\,(1)} = \begin{cases} 0 & \text{if} \quad \tau_{\mathrm{e}}^{(1)} \leq 0, \\ \nu_0^{(1)}\,\exp\Big(-\dfrac{1}{\zeta}\Big)\,\exp\Big(-\dfrac{Q}{k_B\,\vartheta}\Big)\,\left[\sinh\Big(\dfrac{\tau_{\mathrm{e}}^{(1)}\,V}{2k_B\vartheta}\Big)\right]^{1/m^{(1)}} & \text{if} \quad \tau_{\mathrm{e}}^{(1)} > 0, \end{cases} \tag{6.18}$$

where

$$\tau_{\mathrm{e}}^{(1)} \stackrel{\mathrm{def}}{=} \bar{\tau}^{(1)} - (S_a + S_b + \alpha_p\,\bar{p}), \tag{6.19}$$

denotes a *net shear stress for thermally-activated flow*; here $\alpha_p \geq 0$ is a parameter introduced to account for the *pressure sensitivity* of plastic flow. The parameter $\nu_0^{(1)}$ is a *pre-exponential factor* with units of 1/time, Q is an *activation energy*, k_B is Boltzmann's constant, V is an *activation volume*, and $m^{(1)}$ is a *strain rate sensitivity parameter*. The term $\exp(-1/\zeta)$ in (6.18) represents a *concentration of "flow defects,"* where ζ is a dimensionless parameter referred as *normalized equilibrium free-volume* in the literature on amorphous materials.

The thermally activated form for the flow function (6.18) with $\left\{\nu_0^{(1)}, m^{(1)}, \zeta, Q, V\right\}$ *constants*, usually holds over a narrow range of temperatures. Here, in order to model the plastic flow response over a wide range of temperature which spans the glass transition temperature of the material, the parameters ζ and Q *are taken to be temperature dependent*:

- The variation of ζ with temperature is expected to be small for temperatures below ϑ_g. Accordingly we assume that

$$\zeta = \begin{cases} \zeta_{gl} & \text{for } \vartheta \leq \vartheta_g, \\ \zeta_{gl} + d(\vartheta - \vartheta_g) & \text{for } \vartheta > \vartheta_g. \end{cases} \tag{6.20}$$

The simple relation (6.20) is well-defined at temperatures lower than ϑ_g, and has a linear form, similar to the classical Vogel-Fulcher-Tamman (VFT) equation which is used widely to describe the temperature dependence of viscosity of polymeric liquids near their glass transition temperature (Vogel, 1921; Fulcher, 1925; Tammann and Hesse, 1926).[11]

- The temperature dependance of the activation energy Q is taken as

$$Q(\vartheta) = \frac{1}{2}(Q_{gl} + Q_r) - \frac{1}{2}(Q_{gl} - Q_r)\tanh\left(\frac{1}{\Delta}(\vartheta - \vartheta_g)\right), \tag{6.22}$$

where, $Q = Q_{gl}$ in the glassy regime, and $Q = Q_r (< Q_{gl})$ in the rubbery regime.

5. **Evolution equations for internal variables**

Recall that the internal variables $\boldsymbol{\xi}$ have been presumed to evolve according to the differential equations of the form (3.16) in which the functions $\mathcal{R}_i$ represent *static recovery* (or time recovery, or thermal recovery), since they do not depend on the plastic strain rate. The static recovery terms are important in *long time* situations such as creep experiments over a period of hours and days at high temperatures. Here, we focus our attention on recovery processes that occur in relatively shorter periods of time (typically less than 10 minutes), in which case the slow static recovery effects may be neglected. Accordingly, in what follows, as a simplification, we neglect the effects of any static recovery in the evolution of the internal variables.

Evolution of φ and S_a:

We assume that the material disorders, and is accompanied by a microscale dilatation as plastic deformation occurs, resulting in an increase of the order-parameter φ,[12] and this increase in disorder leads to a change in the resistance S_a, causing a transient change in the flow stress of the material as plastic deformation proceeds. Accordingly, the evolution of the resistance S_a is coupled to the evolution of the order-parameter φ. Specifically, we take the evolution of S_a and φ to be governed by

$$\dot{S}_a = h_a\,(S_a^* - S_a)\,\nu^{p(1)}, \qquad \text{with initial value} \qquad S_a(\mathbf{X}, 0) = S_{a0}, \tag{6.23}$$

$$\dot{\varphi} = g\,(\varphi^* - \varphi)\,\nu^{p(1)} \qquad \text{with initial value} \qquad \varphi(\mathbf{X}, 0) = \varphi_0. \tag{6.24}$$

In the evolution equations for S_a and φ, the parameters h_a, g, S_{a0} and φ_0 are constants. During plastic flow, the resistance S_a increases (the material hardens) if $S_a < S_a^*$, and it decreases (the material softens) if $S_a > S_a^*$. The critical value S_a^* of S_a controlling such hardening/softening transitions is assumed to depend on the current values of the plastic strain rate, temperature, and the order-parameter φ. The function S_a^*, which controls the magnitude of the stress-overshoot, is taken as

$$S_a^* = b\,(\varphi^* - \varphi)\,. \tag{6.25}$$

In (6.24), the parameter φ^* represents a strain-rate and temperature dependent critical value for the order-parameter: the material disorders when $\varphi < \varphi^*$, and becomes less disordered if $\varphi > \varphi^*$. Considering the temperature and strain-rate dependence of φ^*, it is expected to decrease with increasing

[11] Instead of the VFT form, other authors (e.g. Richeton et al., 2007; Nguyen et al., 2008) have recently used a Williams-Landel-Ferry (WLF)-type temperature-dependent expression for the plastic shear strain rate to extend to the applicability of their theories to temperatures $\vartheta > \vartheta_g$. The WLF equation (Williams et al., 1955) can be written as

$$\exp\Big(-\frac{1}{\zeta}\Big) = \exp\Big(\frac{(\log_e 10) \times C_1\,(\vartheta - \vartheta_g)}{C_2 + \vartheta - \vartheta_g}\Big), \tag{6.21}$$

where C_1 and C_2 are constants with dimensions of temperature. As is well-known, using suitable manipulations, the VFT and the WLF forms may be shown to be equivalent. Although the WLF and VFT equations are equivalent, the slightly simpler form of the VFT-type equation is often preferred.

[12] The microscale dilatation is extremely small, and at the macroscopic level we presume the plastic flow to be incompressible.

temperature at a fixed strain-rate, and increase with strain-rate at a fixed temperature. We model this temperature and strain rate dependence using the following phenomenological equation

$$\varphi^*(\nu^{p\,(1)},\vartheta)=\begin{cases} z\left(1-\dfrac{\vartheta}{\vartheta_g}\right)^r\left(\dfrac{\nu^{p\,(1)}}{\nu_r}\right)^s & \text{if}\quad (\vartheta\le\vartheta_g)\ \text{ and }\ (\nu^{p\,(1)}>0),\\ 0 & \text{if}\quad (\vartheta>\vartheta_g)\ \text{ or }\ (\nu^{p\,(1)}=0),\end{cases} \tag{6.26}$$

with constants (z,r,s).

Thus, gathering the number of material parameters introduced to phenomenologically model the yield-peak, we have the following rather large list[13]

$$\big(h_a,b,S_{a0},g,\varphi_0,z,r,s\big).$$

Evolution of S_b:

Our experiments above ϑ_g indicate that the non-linear stress response at large strains is not purely elastic as the unloading response shows significant hysteresis. It is for this reason that we have introduced the internal variable S_b to model a *dissipative* resistance to plastic flow which arises as the chains are pulled taut between entanglements, and there is increasing interaction between the long-chain molecules and pendant side-groups; this resistance is *in addition* to any entropic contribution from network chain-stretching. For the resistance S_b we assume

$$S_b=S_{b0}+H_b(\bar\lambda-1)^\ell, \tag{6.27}$$

where

$$\bar\lambda\stackrel{\text{def}}{=}\sqrt{\operatorname{tr}\mathbf{C}/3}\equiv\sqrt{\mathbf{C}^{e\,(1)}:\mathbf{B}^{p\,(1)}/3} \tag{6.28}$$

is an *effective stretch* which increases or decreases as the overall stretch increases or decreases. In (6.27) the material parameter H_b is temperature dependent:

$$H_b(\vartheta)=\frac{1}{2}\left(H_{gl}+H_r\right)-\frac{1}{2}\left(H_{gl}-H_r\right)\tanh\Big(\frac{1}{\Delta}(\vartheta-\vartheta_g)\Big)-L(\vartheta-\vartheta_g), \tag{6.29}$$

where H_{gl} and H_r $(<H_{gl})$ are values of H_b in the glassy and rubbery regions near the glass transition temperature ϑ_g, and L represents the slope of the temperature variation of H_b beyond the glass transition region, with

$$L=\begin{cases} L_{gl} & \vartheta\le\vartheta_g,\\ L_r & \vartheta>\vartheta_g.\end{cases} \tag{6.30}$$

6.2 Constitutive equations for micromechanism $\alpha=2$

1. **Free energy**

   Let

$$\mathbf{F}^{e\,(2)}_{\text{dis}}\stackrel{\text{def}}{=}J^{-1/3}\,\mathbf{F}^{e(2)},\quad \det\mathbf{F}^{e\,(2)}_{\text{dis}}=1, \tag{6.31}$$

   denote the distortional part of $\mathbf{F}^{e(2)}$. Correspondingly, let

$$\mathbf{C}^{e\,(2)}_{\text{dis}}\stackrel{\text{def}}{=}(\mathbf{F}^{e\,(2)}_{\text{dis}})^\top\mathbf{F}^{e\,(2)}_{\text{dis}}=J^{-2/3}\mathbf{C}^{e(2)}, \tag{6.32}$$

   denote the elastic distortional right Cauchy-Green tensor and consider a free energy function in the special form[14]

$$\psi^{(2)}=\bar\psi^{(2)}(\mathbf{C}^{e\,(2)}_{\text{dis}},\vartheta), \tag{6.33}$$

[13] Modeling the temperature and rate-sensitivity of the yield-peak over a wide-range of temperatures and strain rates is known to be complex. If a simpler theory with fewer material parameters is desired, and if it is deemed that modeling the yield-peak is not of interest, then there is no need to introduce the internal variables φ and S_a, and thereby also the attendant constants in their evolution equations.

[14] Since $J^{e\,(\alpha)}=J$, and we have already accounted for a volumetric elastic energy for $\psi^{(1)}$, we do not allow for a volumetric elastic energy for $\psi^{(2)}$ or $\psi^{(3)}$.

with $\bar{\psi}^{(2)}(\mathbf{C}^{e\,(2)}_{\rm dis}, \vartheta)$ an isotropic function of its arguments. We use a simple phenomenological form for the free energy function $\psi^{(2)}$ proposed by Gent (1996)[15]:

$$\psi^{(2)} = -\tfrac{1}{2}\mu^{(2)}\, I_m^{(2)}\, \ln\Big(1 - \frac{I_1^{(2)} - 3}{I_m^{(2)}}\Big), \qquad \text{with} \qquad I_1^{(2)} \stackrel{\rm def}{=} \operatorname{tr} \mathbf{C}^{e\,(2)}_{\rm dis}, \tag{6.34}$$

where

$$\mu^{(2)}(\vartheta) > 0 \qquad \text{and} \qquad I_m^{(2)}(\vartheta) > 3 \tag{6.35}$$

are two temperature-dependent material constants, with $\mu^{(2)}$ representing the ground state rubbery shear modulus of the material, and $I_m^{(2)}$ represents a maximum value of $(I_1^{(2)} - 3)$ associated with the limited extensibility of the polymer chains.

Experimental results indicate that the rubbery shear modulus $\mu^{(2)}$ *decreases* with increasing temperature; the empirical function chosen to fit the experimentally-observed temperature dependence of $\mu^{(2)}$ is

$$\mu^{(2)}(\vartheta) = \mu_g^{(2)}\, \exp\Big(-N(\vartheta - \vartheta_g)\Big), \tag{6.36}$$

where $\mu_g^{(2)}$ is the value of $\mu^{(2)}$ at the glass transition temperature, and N is a parameter that represents the slope of temperature variation on a logarithmic scale. The parameter $I_m^{(2)}$ is taken to be temperature-independent constant

$$I_m^{(2)}(\vartheta) \approx \text{constant}. \tag{6.37}$$

2. **Cauchy stress. Mandel stress**

The free energy (6.34) yields the corresponding second Piola stress as

$$\mathbf{S}^{e(2)} = 2\frac{\partial \psi^{(2)}}{\partial \mathbf{C}^{e(2)}} \tag{6.38}$$

$$= J^{-2/3}\mu^{(2)}\left(1 - \frac{I_1^{(2)} - 3}{I_m^{(2)}}\right)^{-1}\left[\mathbf{1} - \frac{1}{3}\left(\operatorname{tr}\mathbf{C}^{e\,(2)}_{\rm dis}\right)\mathbf{C}^{e(2)\,-1}_{\rm dis}\right], \tag{6.39}$$

which gives a deviatoric contribution $\mathbf{T}^{(2)}$ to the Cauchy stress as

$$\mathbf{T}^{(2)} = J^{-1}\mathbf{F}^{e(2)}\mathbf{S}^{e(2)}\mathbf{F}^{e(2)\top} \tag{6.40}$$

$$= J^{-1}\left[\mu^{(2)}\left(1 - \frac{I_1^{(2)} - 3}{I_m^{(2)}}\right)^{-1}(\mathbf{B}^{e\,(2)}_{\rm dis})_0\right], \tag{6.41}$$

where

$$\mathbf{B}^{e\,(2)}_{\rm dis} \stackrel{\rm def}{=} \mathbf{F}^{e\,(2)}_{\rm dis}(\mathbf{F}^{e\,(2)}_{\rm dis})^{\top} = J^{-2/3}\mathbf{B}^{e\,(2)} \tag{6.42}$$

denotes the elastic distortional left Cauchy-Green tensor.

The corresponding (deviatoric) Mandel stress is

$$\mathbf{M}^{e(2)} = \mathbf{C}^{e(2)}\mathbf{S}^{e(2)} = \mu^{(2)}\left(1 - \frac{I_1^{(2)} - 3}{I_m^{(2)}}\right)^{-1}(\mathbf{C}^{e\,(2)}_{\rm dis})_0, \tag{6.43}$$

and the *equivalent shear stress* for plastic flow is given by

$$\bar{\tau}^{(2)} \stackrel{\rm def}{=} \frac{1}{\sqrt{2}}\,|\mathbf{M}^{e(2)}|. \tag{6.44}$$

[15]There is a conceptual difficulty with using statistical-mechanical ideas of the theory of entropic rubber elasticity to describe the strain hardening due to chain-stretching at temperatures below the glass transition temperature, because at these temperatures the chains do not have sufficient mobility to sample all possible molecular conformations. The phenomenological Gent free energy function has been shown by Boyce (1996) to yield predictions for the stress-strain response similar to the entropic-network model of Arruda and Boyce (1993).

3. **Flow rule. Internal variables**

The evolution equation for $\mathbf{F}^{p(2)}$ is

$$\dot{\mathbf{F}}^{p\,(2)} = \mathbf{D}^{p(2)}\,\mathbf{F}^{p(2)}, \tag{6.45}$$

with the plastic stretching $\mathbf{D}^{p(2)}$ given by

$$\mathbf{D}^{p(2)} = \nu^{p(2)}\left(\frac{\mathbf{M}^{e\,(2)}}{2\bar{\tau}^{(2)}}\right), \qquad \text{where} \quad \nu^{p(2)} \stackrel{\text{def}}{=} \sqrt{2}|\mathbf{D}^{p(2)}| \tag{6.46}$$

is the corresponding equivalent plastic shear strain rate. With $S^{(2)}(\vartheta)$ a positive-valued stress-dimensioned shear resistance, we take the equivalent plastic strain rate to be

$$\nu^{p(2)} = \nu_0^{(2)}\left(\frac{\bar{\tau}^{(2)}}{S^{(2)}}\right)^{1/m^{(2)}}, \tag{6.47}$$

where $\nu_0^{(2)}$ is a reference plastic shear strain rate and $m^{(2)}$ is a positive-valued strain-rate sensitivity parameter.

We assume that $S^{(2)}$ varies with temperature as

$$S^{(2)}(\vartheta) = \tfrac{1}{2}(S_{gl}^{(2)} + S_r^{(2)}) - \tfrac{1}{2}(S_{gl}^{(2)} - S_r^{(2)})\tanh\Big(\frac{1}{\Delta_2}(\vartheta - \vartheta_g)\Big), \tag{6.48}$$

where, $S^{(2)} = S_{gl}^{(2)}$ in the glassy regime, and $S^{(2)} = S_r^{(2)} (\ll S_{gl}^{(2)})$ in the rubbery regime, and Δ_2 is a parameter related to the temperature range across which the transition occurs. A high value of $S^{(2)} = S_{gl}^{(2)}$ leads to $\nu^{p(2)} \approx 0$ when $\vartheta < \vartheta_g$, and as the temperature increases through the glass transition, the value of $S^{(2)}$ smoothly transitions to a very low value, allowing for plastic flow above ϑ_g. This assumption is meant to reflect the major effect of the rapid destruction of a *large fraction* of mechanical cross-links as the temperature increases beyond ϑ_g. To ensure a very rapid transition of $S^{(2)}$ near ϑ_g, we take $\Delta_2 = \Delta/20$. Thus, under a macroscopically-imposed deformation history at temperatures greater than a few degrees higher than ϑ_g, micromechanism $\alpha = 2$ freely deforms inelastically by relative chain-slippage, and there is no further increase in the corresponding elastic stretch $\mathbf{U}^{e\,(2)}$, and thereby the corresponding stress.

6.3 Constitutive equations for micromechanism $\alpha = 3$

1. **Free energy**

Let

$$\mathbf{F}_{\text{dis}} \stackrel{\text{def}}{=} J^{-1/3}\,\mathbf{F}, \quad \det\mathbf{F}_{\text{dis}} = 1, \tag{6.49}$$

denote the distortional part of $\mathbf{F}$. Correspondingly, let

$$\mathbf{C}_{\text{dis}} \stackrel{\text{def}}{=} (\mathbf{F}_{\text{dis}})^{\top}\mathbf{F}_{\text{dis}} = J^{-2/3}\mathbf{C}, \tag{6.50}$$

denote the distortional right Cauchy-Green tensor, and consider a free energy function in the special form

$$\psi^{(3)} = \bar{\psi}^{(3)}(\mathbf{C}_{\text{dis}}, \vartheta). \tag{6.51}$$

Similar to the case $\alpha = 2$, we assume the free energy in the Gent form as

$$\psi^{(3)} = -\tfrac{1}{2}\mu^{(3)}\,I_m^{(3)}\,\ln\Big(1 - \frac{I_1^{(3)} - 3}{I_m^{(3)}}\Big), \qquad \text{with} \qquad I_1^{(3)} \stackrel{\text{def}}{=} \operatorname{tr}\mathbf{C}_{\text{dis}}, \tag{6.52}$$

where

$$\mu^{(3)} > 0, \qquad \text{and} \qquad I_m^{(3)} > 3 \tag{6.53}$$

are two material constants. These two material constants are assumed to be *temperature-independent*.

2. **Cauchy stress**

Using the free energy (6.52) yields the corresponding second Piola stress as

$$\mathbf{S}^{e\,(3)} = J^{-2/3}\mu^{(3)}\left(1-\frac{I_1^{(3)}-3}{I_m^{(3)}}\right)^{-1}\left[\mathbf{1}-\frac{1}{3}\left(\operatorname{tr}\mathbf{C}_{\rm dis}\right)\mathbf{C}_{\rm dis}^{-1}\right], \tag{6.54}$$

and the contribution $\mathbf{T}^{(3)}$ to Cauchy stress as

$$\mathbf{T}^{(3)} = J^{-1}\left[\mu^{(3)}\left(1-\frac{I_1^{(3)}-3}{I_m^{(3)}}\right)^{-1}(\mathbf{B}_{\rm dis})_0\right], \tag{6.55}$$

where

$$\mathbf{B}_{\rm dis} \stackrel{\rm def}{=} \mathbf{F}_{\rm dis}(\mathbf{F}_{\rm dis})^{\top} = J^{-2/3}\mathbf{B} \tag{6.56}$$

denotes the distortional left Cauchy-Green tensor.

6.4 Partial differential equation for the temperature field

At this stage of the specialization of the theory, since very little is experimentally known about the variation of specific heat with elastic deformation (cf., (3.22)), viz.

$$c \stackrel{\rm def}{=} -\vartheta\sum_{\alpha}\frac{\partial^2\bar{\psi}^{e\,(\alpha)}(\mathcal{I}_{\mathbf{C}^{e\,(\alpha)}},\vartheta)}{\partial\vartheta^2},$$

we assume (i) that the specific heat depends only on temperature, $c \approx \hat{c}(\vartheta)$; and (ii) we also neglect the thermoelastic coupling terms in (3.23), viz.

$$\vartheta\sum_{\alpha}\frac{\partial^2\bar{\psi}^{e(\alpha)}}{\partial\vartheta\,\partial\mathbf{C}^{e\,(\alpha)}}:\dot{\mathbf{C}}^{e\,(\alpha)}.$$

To compensate for these approximative assumptions, we assume instead that only a fraction $0 \lessapprox \omega \lessapprox 1$ of the rate of plastic dissipation contributes to the temperature changes. Under these assumptions, the simplified partial differential equation for the temperature becomes

$$c\dot{\vartheta} = -\operatorname{Div}\mathbf{q}_{\rm R} + q_{\rm R} + \omega\left(\bar{\tau}^{(1)}\,\nu^{p\,(1)} + \bar{\tau}^{(2)}\,\nu^{p\,(2)}\right). \tag{6.57}$$

Table 1: Material parameters

Parameter	Value	Parameter	Value
ρ (kg m^{-3})	1020	b (MPa)	5850
α_{gl} (K^{-1})	13×10^{-5}	g	5.8
α_r (K^{-1})	25×10^{-5}	φ_0	0
ν_r (s^{-1})	5.2×10^{-4}	z	0.083
ϑ_r (K)	310	r	1.3
n (K)	2.1	s	0.005
Δ (K)	2.6	S_{b0} (MPa)	0
G_{gl} (MPa)	156	$H_{gl}(MPa)$	1.56
G_r (MPa)	13.4	L_{gl} (MPa K^{-1})	0.44
M_{gl} (MPa K^{-1})	7.4	H_r (MPa)	0.76
M_r (MPa K^{-1})	0.168	L_r (MPa K^{-1})	0.006
ν_{gl}^{poi}	0.35	l	0.5
ν_r^{poi}	0.49	$\mu_g^{(2)}$ (MPa)	1.38
α_p	0.058	N (K^{-1})	0.045
$\nu_0^{(1)}$ (s^{-1})	1.73×10^{13}	$I_m^{(2)}$	6.3
$m^{(1)}$	0.17	$\nu_0^{(2)}$ (s^{-1})	5.2×10^{-4}
V (m^3)	2.16×10^{-27}	$m^{(2)}$	0.19
Q_{gl} (J)	1.4×10^{-19}	$S_{gl}^{(2)}$ (MPa)	58
Q_r (J)	0.2×10^{-21}	$S_r^{(2)}$ (MPa)	3 $\times 10^{-4}$
ζ_{gl}	0.14	$\mu^{(3)}$ (MPa)	0.75
d (K^{-1})	0.015	$I_m^{(3)}$	5.0
S_{a0} (MPa)	0	ω	0.7
h_a	230		

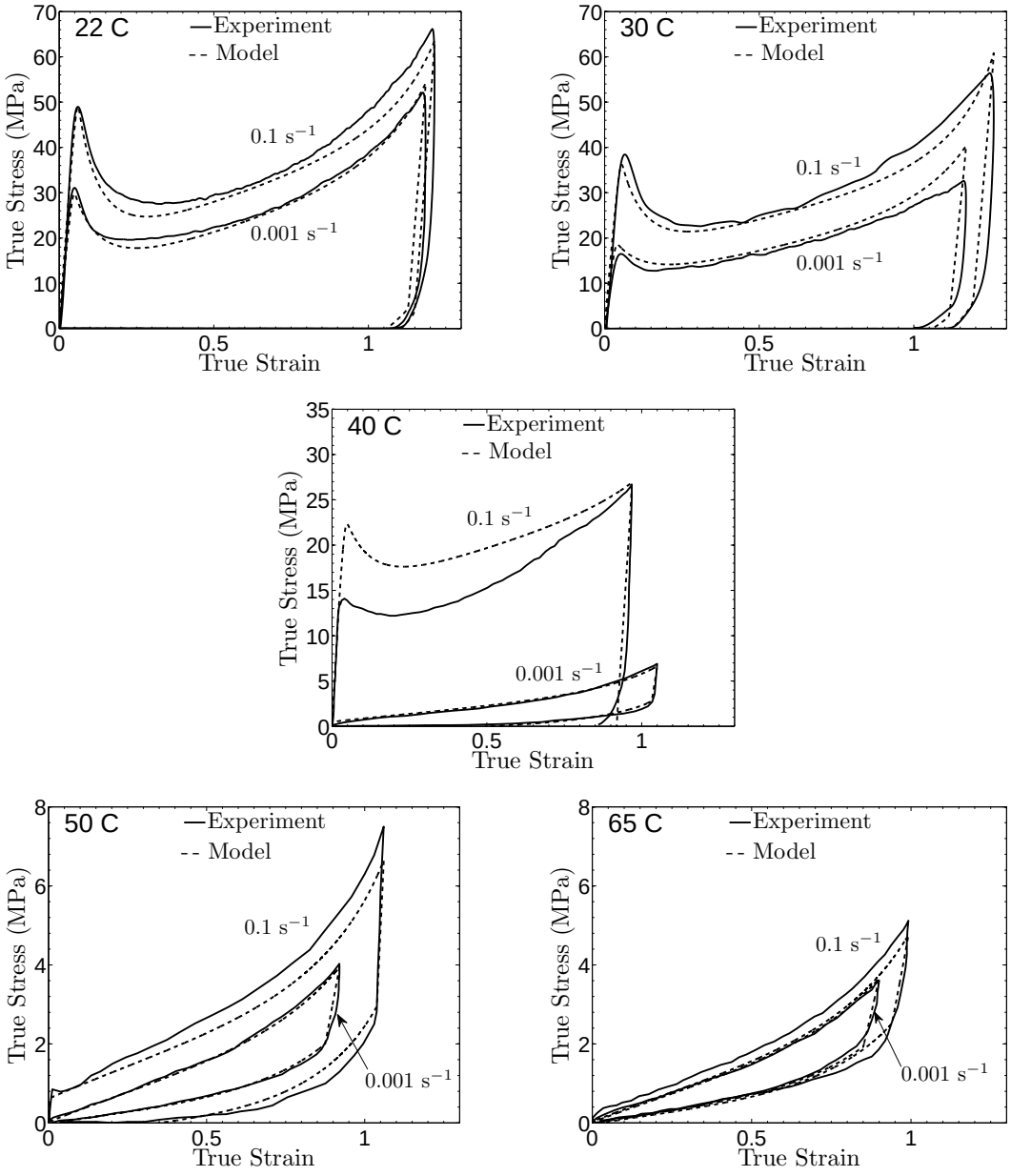

Figure 1: Stress-strain curves in simple compression for the shape-memory polymer at strain rates of $10^{-3}\,\mathrm{s}^{-1}$ and $10^{-1}\,\mathrm{s}^{-1}$, and at temperatures of 22 C, 30 C, 40 C, 50 C, and 65 C. The figure also shows the fit of our constitutive model to experimental stress-strain curves. The experimental data is plotted as solid lines, while the fit is shown as dashed lines. Note the change in scale for the stress axis between various figures.

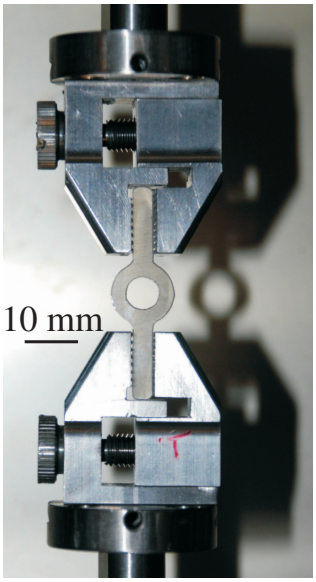

Figure 2: Experimental set-up for a thermo-mechanical constrained-recovery experiment on a ring-shaped specimen of tBA/PEGDMA.

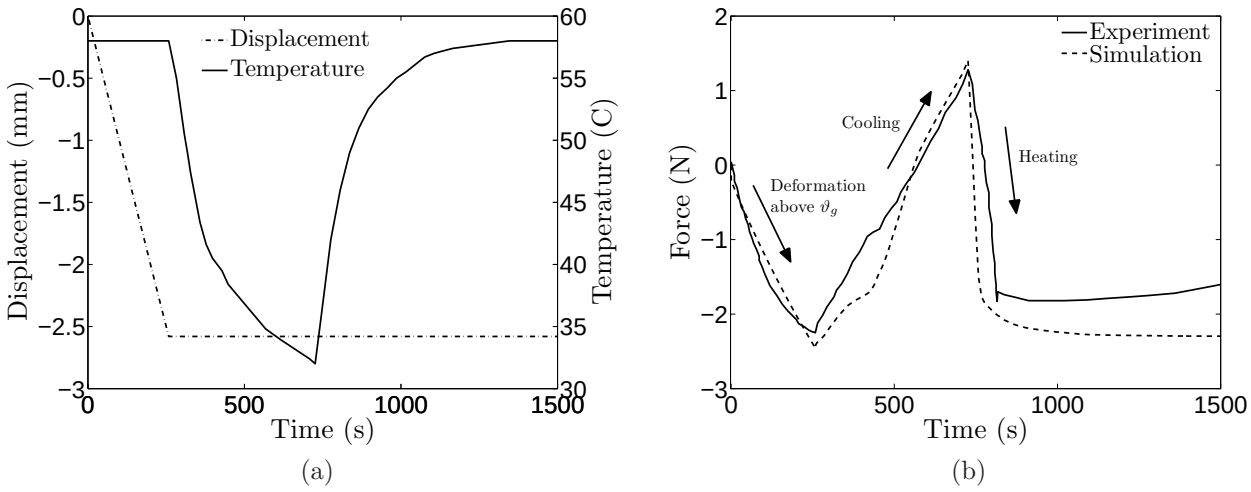

Figure 3: (a) Histories of the specimen-temperature and the relative-displacement of the grips: the specimen, initially at 58 C, was compressed and the grips were then fixed in position while the specimen was first cooled to 32 C and then heated back to 58 C; corresponding reaction forces were measured by a load-cell. (b) The solid line shows the experimentally-measured force-versus-time curve for the constrained-recovery experiment. The corresponding numerically-predicted response is shown as a dashed line.

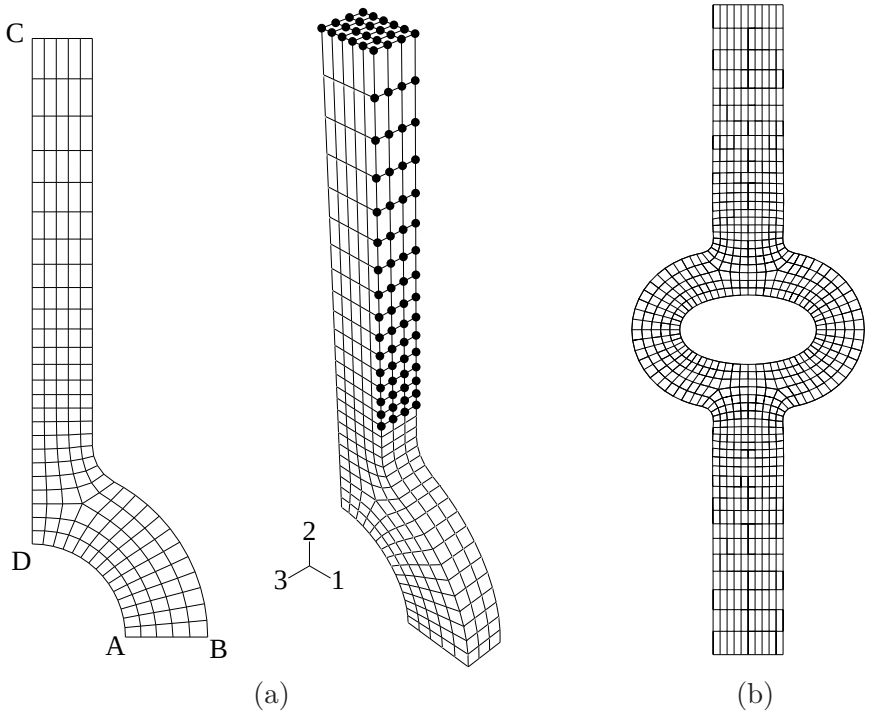

Figure 4: (a) One-eighth symmetry finite element mesh for the ring-shaped polymer. All the nodes on the surface formed by CD extending into the 3-direction were prescribed symmetry in the 1-direction, all the nodes on the surface formed by AB extending into the 3-direction were prescribed symmetry in the 2-direction, and all the nodes on the front surface defined by ABCD were prescribed symmetry in the 3-direction. A displacement history was prescribed to the highlighted nodes on the outer surface of the extension arm such that the displacement history for the complete geometry matched that of the experiment in Fig. 4b. (b) Deformed mesh.

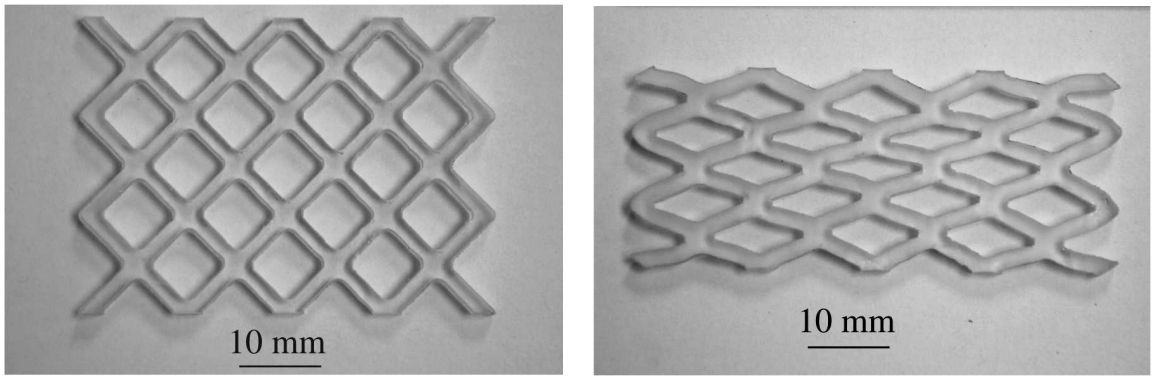

(a) (b)

Figure 5: Diamond-lattice-shaped specimen: (a) Undeformed specimen. (b) Deformed specimen in its "temporary shape" at room temperature — deformed at 60 C, constrained cooling to 21 C, and constraints removed.

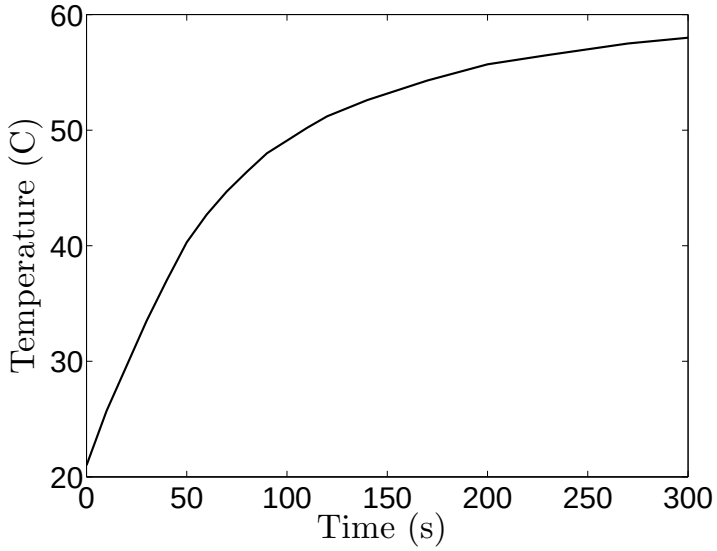

Figure 6: Time-temperature history for the diamond-lattice-shaped specimen during the unconstrained heating phase of the experiment.

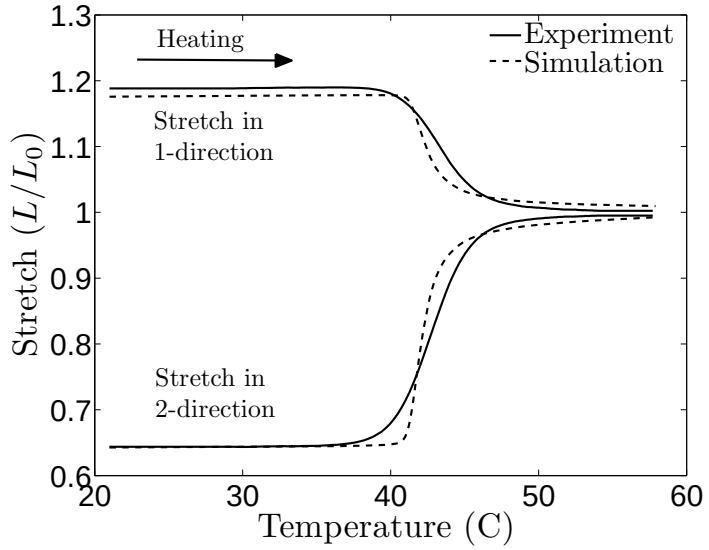

Figure 7: The solid lines show the experimentally-measured stretch-versus-temperature curves in the 1- and 2-direction during the unconstrained heating phase of the experiment. The dashed-lines are the corresponding numerically-predicted results.

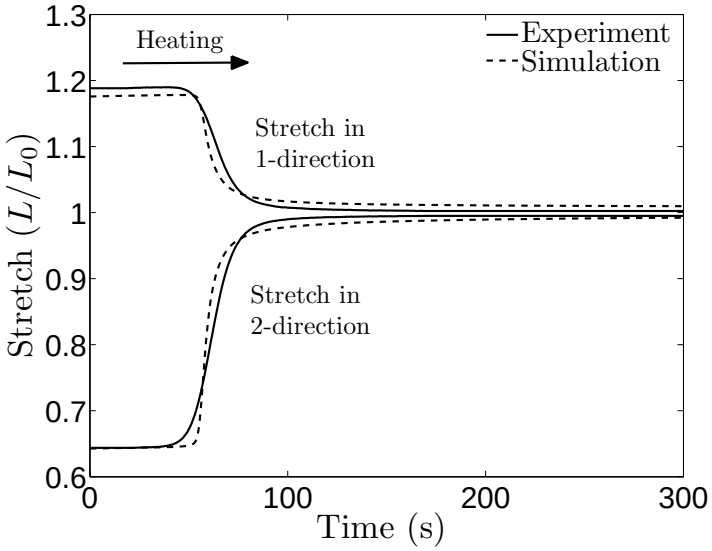

Figure 8: The solid lines show the experimentally-measured stretch-versus-time curves in the 1- and 2-direction during the unconstrained heating phase of the experiment. The dashed-lines are the corresponding numerically-predicted results.

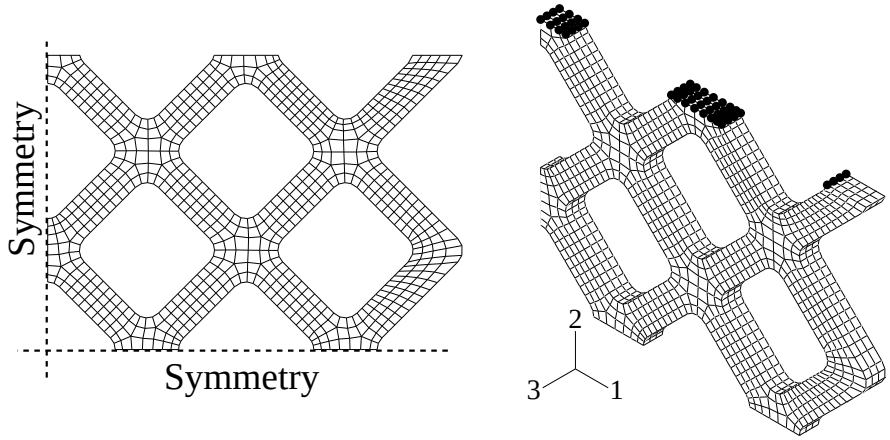

Figure 9: One-eighth symmetry finite element mesh for the diamond-shaped lattice geometry. All the nodes on the symmetry plane 2-3 were prescribed symmetry in the 1-direction, all the nodes on the symmetry plane 1-3 were prescribed symmetry in the 2-direction, and all the nodes on the front surface were prescribed symmetry in the 3-direction. A displacement history was prescribed to the highlighted nodes on the top surface to obtain a temporary shape that closely matches that from the experiment.

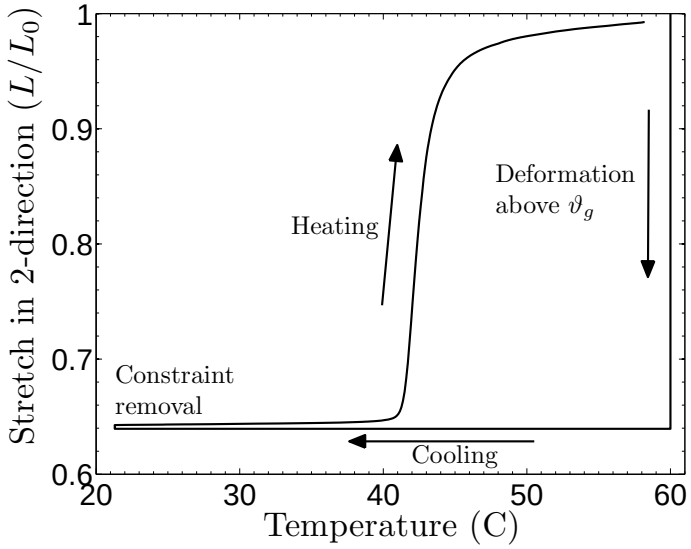

Figure 10: Numerical simulation results for the complete thermo-mechanical shape-recovery cycle of the lattice geometry. The lattice was deformed in the 2-direction at 60 C; after which it was constrained in the 2-direction and was cooled to 21 C; the constraints were then removed which resulted in a small elastic recovery; finally, the lattice was heated to 58 C during which, it recovered almost to its original shape.

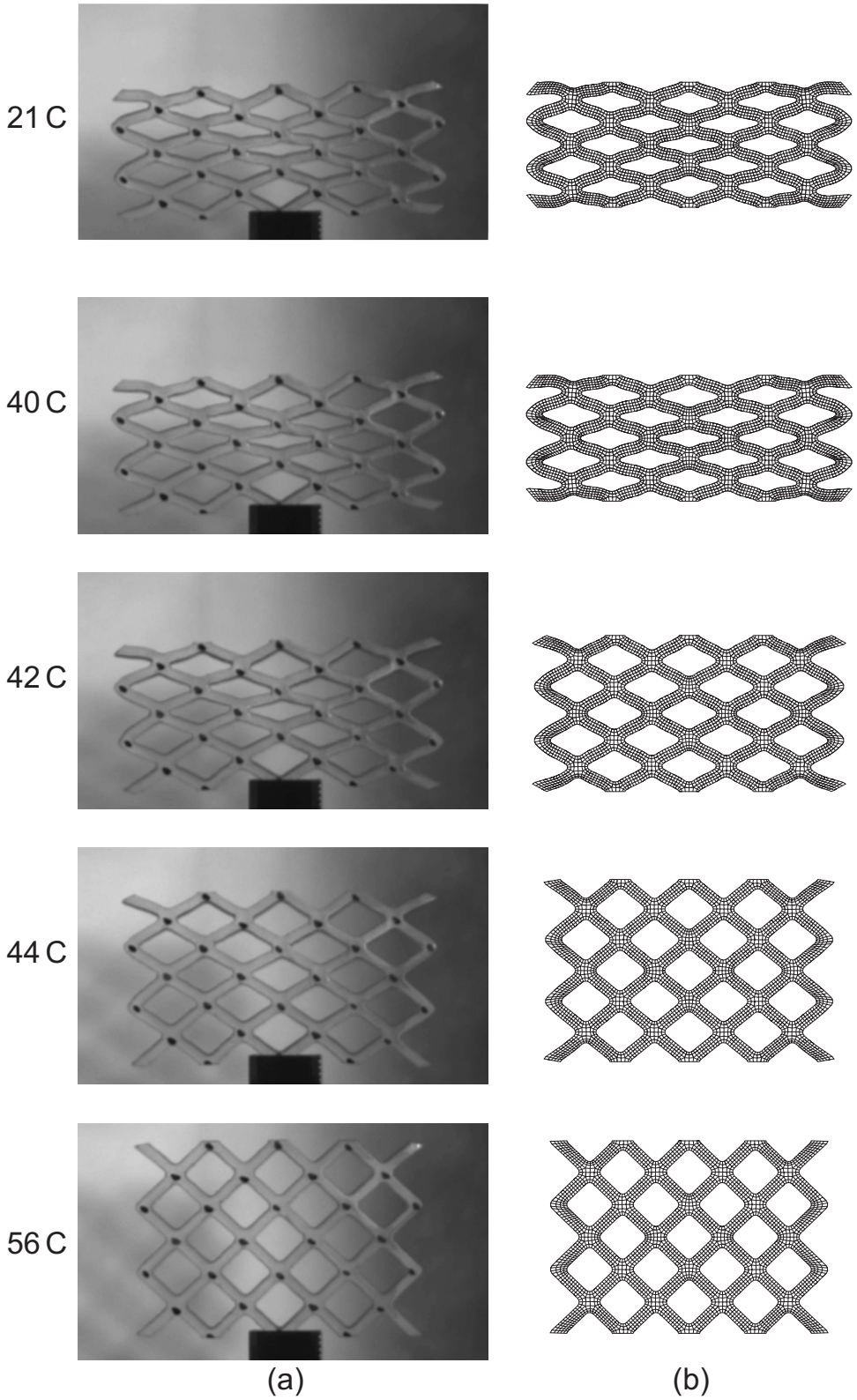

Figure 11: Comparison of (a) the experimentally-observed, and (b) the numerically-predicted recovered shapes at various temperatures during the unconstrained-recovery phase of the experiment.

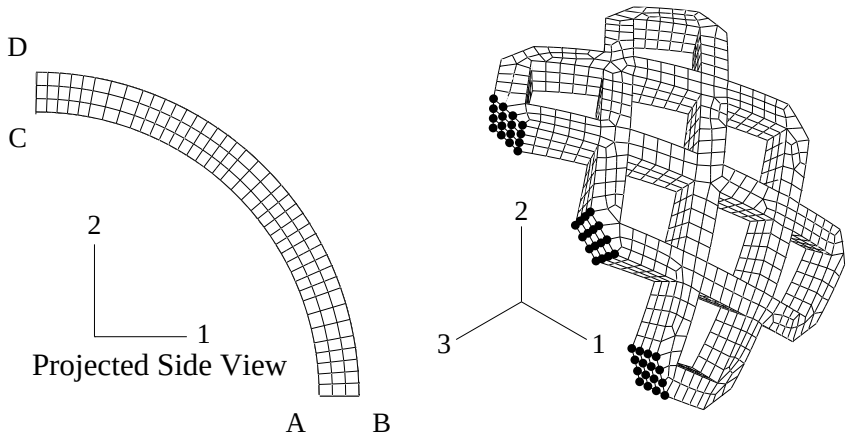

Figure 12: One-eighth symmetry finite element mesh for a vascular stent. The displacement boundary conditions prescribed were: symmetry in the 1-direction for the nodes on the surface formed by edge CD extending into the 3-direction; symmetry in the 2-direction for the nodes on the surface defined by edge AB extending into the 3-direction; and symmetry in the 3-direction for the highlighted nodes on the front surface.

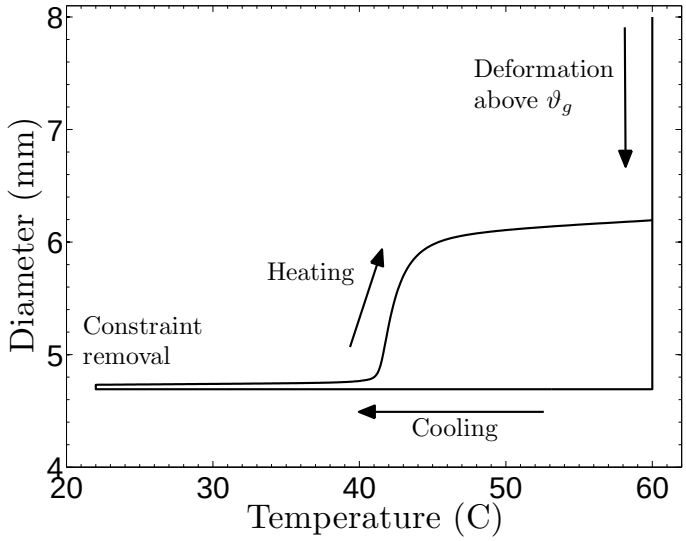

Figure 13: Predictions from the numerical simulation for the outer-diameter of the stent at different temperatures during the imposed thermo-mechanical history of insertion of a stent in an artery: (i) the tBA/PEGDMA stent was radially compressed at 60 C to reduce its outer diameter from its initial 8 mm value to 4.7 mm; (ii) the compressed stent was cooled to 22 C; (iii) the constraints were then removed and the stent recovered to a diameter of 4.74 mm at 22 C; finally (iv) the stent was inserted into an artery and was heated to 60 C during which its outer diameter recovered to a value of 6.22 mm.

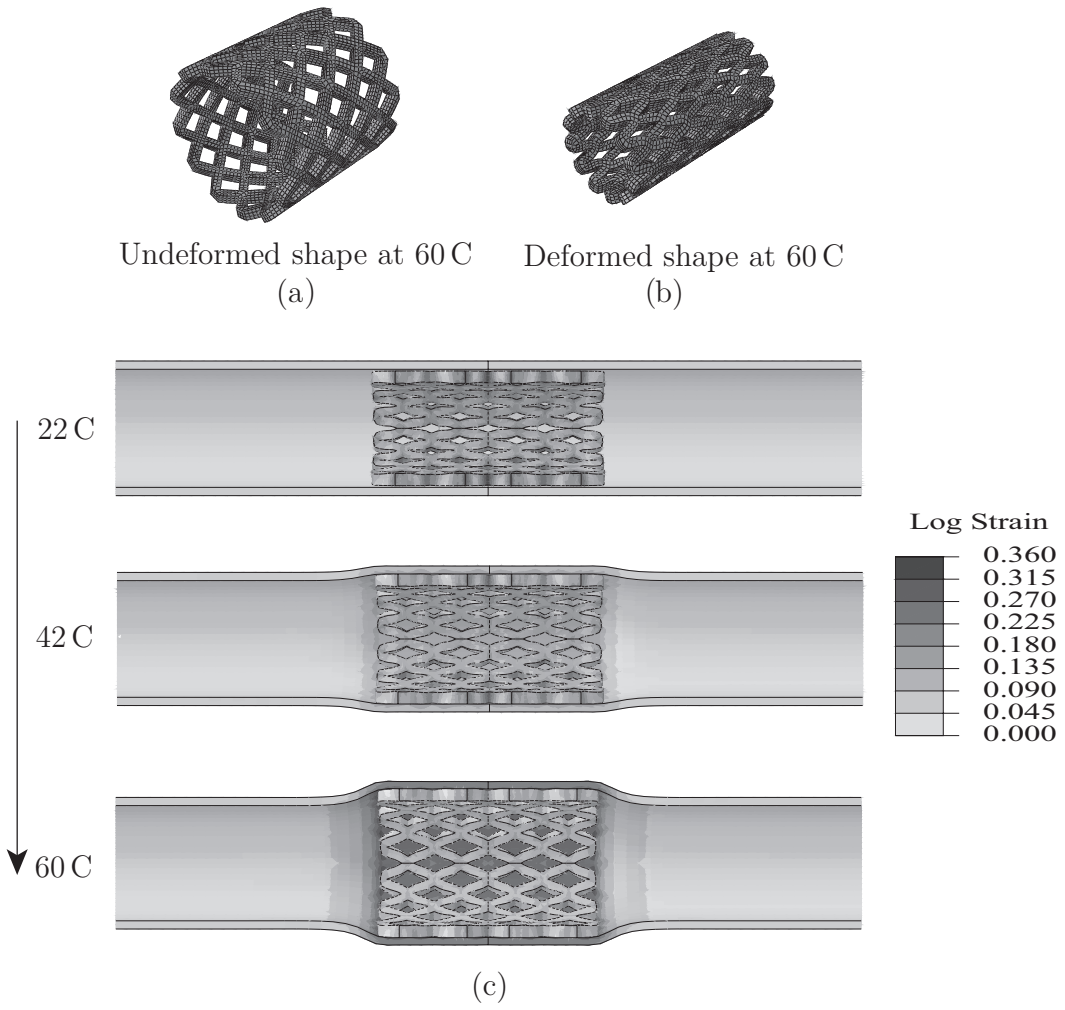

Figure 14: Numerically-predicted thermo-mechanical shape-recovery cycle for the vascular stent; for clarity the mesh has been mirrored along relevant symmetry planes to show the full stent and artery. (a) Undeformed original stent. (b) Deformed stent. (c) Shape-recovery of the stent inside the artery with temperature.

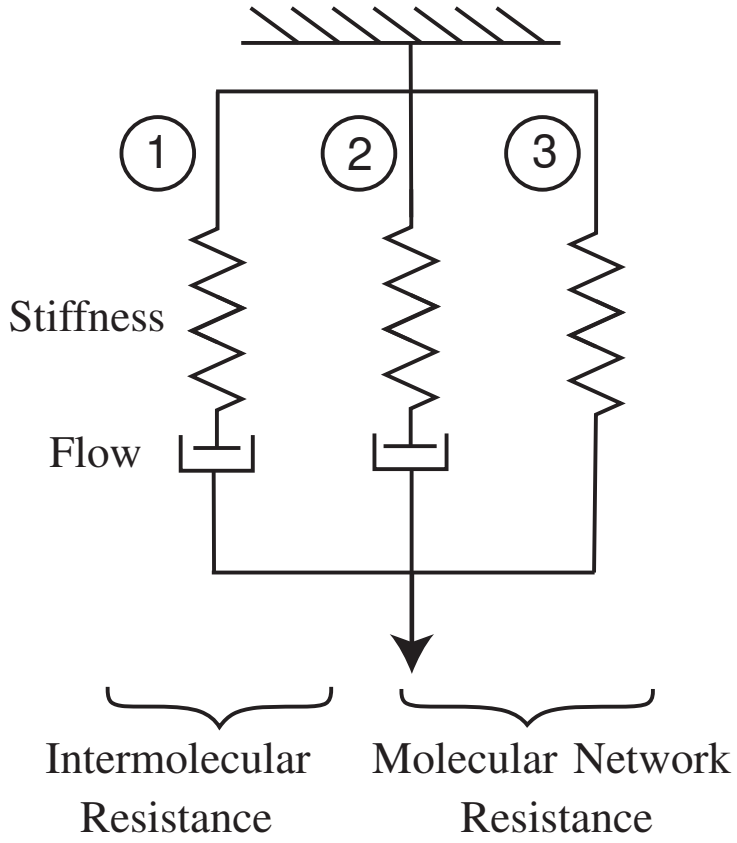

Figure 15: A schematic "spring-dashpot" representation of the constitutive model.